nature communications

Article

https://doi.org/10.1038/s41467-025-59622-4

Blocking plasma cell fate enhances antigen-specific presentation by B cells to boost anti-tumor immunity

Received: 28 August 2024

Accepted: 30 April 2025

Published online: 14 May 2025

Check for updates

Yunqiao Li[1], Raag Bhargava[1], Jenny Tuyet Tran[1], Tanya R. Blane[1], Linghang Peng[1], Fangkun Luan[1], Zhe Huang[1], Zefan Zhang[2], Yunfan Sun[2], Changchun Xiao[1] ✉ & David Nemazee[1] ✉

B cells engage in anti-tumor immunity but how they contribute to cancer suppression remains unclear. We report that inhibiting plasma cell differentiation either in IgMi mice lacking *Igh* elements needed for antibody secretion or in mice with B cell-specific knockout of Blimp-1 (Blimp-1 BcKO) promotes rather than inhibits antitumor immunity and increases numbers of activated B cells. Deficiency of Blimp-1 in tumor-infiltrating B cells generates a unique transcription profile associated with expansion of mutated clones targeting cognate tumor cells. Major histocompatibility complex class II (MHC II) is required for anti-tumor efficacy. Blimp-1-deficient B cells have increased expression of CD80 and CD86 costimulatory molecules that enhance effector T cell function. The Blimp-1 inhibitor valproic acid suppresses tumor growth in a B cell-dependent manner. Thus, inhibition of plasma cell differentiation results in enhanced tumor-specific antigen presentation by B cells and thereby tumor repression, suggesting a potential avenue of immunotherapy against cancer.

The function of B cells in tumors is controversial[1,2]. Naïve B cells enter the secondary lymphoid structures, proliferate, form germinal centers (GCs), and undergo immunoglobulin class switch after antigen (Ag) stimulation. GC B cells (GCB) produce cytokines, present antigens, and differentiate into antibody-secreting plasma cells (PC) or memory B cells (MBCs). In the serum of cancer patients, elevated levels of antibodies against tumor-associated antigens (TAAs) are often detected, assisting cancer diagnosis[3–5]. Antigen-specific antibody secreting cells can be found in the tumor microenvironment as well[6]. The presence of B cells in the tumor microenvironment correlates with favorable prognosis in ovarian cancer[7], breast cancer[8], and neuroblastoma[9]. Tumor-infiltrating B cell (TIL-B)-enriched tumors with expansion of IgG isotype was associated with improved survival outcomes in aggressive triple-negative breast cancers[10]. Antigen recognition by tumor-specific IgA isotypes contribute to suppression of ovarian carcinoma malignant progression[11]. Conversely, it has been reported that increased intestinal B cells and their IgA secretions mediate metabolic T-cell activation and fibrosis which is a high risk for hepatocellular carcinoma (HCC)[12]. HCC tumor-derived dendritic cells activate IL-10-expressing B cells to suppress CD8 T cell function[13]. In addition to IL-10, regulatory B (Breg) cells express other immune-suppressive cytokines including transforming growth factor-β and IL-35 to maintain immune homeostasis in various tissues; when dysregulated, Breg cells may cause autoimmunity, allergic diseases, and cancer[14]. Autoantibodies secreted by B cells cause deposition of immune complexes within squamous cell carcinogenesis tissues that activates Fcγ receptor (FcγR)-mediated protumor pathways in mast cells and T helper (T_H) 2-tumor-associated macrophages[15]. In HCC tissues, IgG produced by CXCL10-stimulated TIL-Bs interacts with FcγR on macrophages to reduce anti-tumor immunity[16]. TIL-Bs can colocalize with T cells and

[1]Department of Immunology and Microbiology, The Scripps Research Institute, La Jolla, CA, USA. [2]Department of Liver Surgery & Transplantation, Liver Cancer Institute, Zhongshan Hospital, Fudan University, Key Laboratory of Carcinogenesis and Cancer Invasion, Ministry of Education, Shanghai, China. ✉e-mail: cxiao@scripps.edu; nemazee@scripps.edu

follicular dendritic cells in tertiary lymphoid structures (TLSs) to promote T cell responses[17]. In contrast to dendritic cells, which are critical for T cell priming, B cells are recruited into tumor microenvironments to promote tumor-specific T cell expansion and memory T cell formation[18]. Moreover, B cells can recognize neoantigens and promote T follicular helper cell (Tfh) differentiation, which enhances effector CD8 T cell functions by producing IL-21[19]. These studies indicate that TIL-Bs participate in a variety of tumor-specific local immune responses.

The mechanism by which B cells might promote tumor suppression, through the production of tumor specific antibodies or through antigen presentation to T cells, is difficult to address in human beings because both processes occur concurrently. For specific antibodies to be formed, B cells must first interact with antigen and cognate CD4 T cells in GCs or TLSs. Antibody formation normally occurs only after considerable clonal expansion and often after processes such as somatic mutation or heavy chain class switching. B cells also play a unique role in presenting antigen to T cells, indeed they are often crucial for presentation of foreign antigen to T cells[20,21], probably because of their unique ability to take up specific antigen via the B cell receptor[22,23]. But their role in cancer is less clear because B cell presentation of self-antigens can be tolerogenic or suppressive[24,25]. To address the extent to which cancer repression involves anti-tumor antibodies, as opposed to B cell antigen presentation to T cells, we have studied the effects in mice of blocking PC differentiation.

PC differentiation and immunoglobulin secretion critically require Blimp-1[26]. Blimp-1 also inhibits cell proliferation by negatively regulating c-Myc, promoting quiescence of activated B cells and retarding their apoptosis[27]. In *Prdm1*$^{fl/fl}$ CD19cre mice, which lack Blimp-1 specifically in B cells, PC development and antibody secretion are blocked, but germinal center reactions are intact[28]. Tumor challenge of B cell-restricted Blimp-1-deficient mice thus allows one to dissect the contribution of tumor-infiltrating B cells to tumor suppression in the absence of antibody secretion. Similarly, IgMi mice, which show normal B cell development and maturation but lack class switch recombination and antibody secretion during immune responses[29] provide an independent model precluding antibody secretion.

In this study, we show that blocking PC differentiation aids, rather than hinders tumor resistance. We also explore the dynamics and antigen recognition of tumor-infiltrating B cells via single-cell (sc) transcriptomic and 5′V(D)J sequencing, through which we demonstrate a pathway that promotes effector T cell responses and tumor suppression by enhancing in situ tumor-specific antigen presentation and costimulation by B cells.

Results

Blimp-1 deficiency in B cells promotes antitumor immunity

Total IgG1 levels were strikingly increased upon inoculation in syngeneic mice of colorectal adenocarcinoma cell line MC38 (Supplementary Fig. 1a), leading us to investigate the functions of PCs and antibodies in tumor immunity. We found that IgMi mice had a striking tumor repression phenotype (Fig. 1a and Supplementary Fig. 1b, c), suggesting that antibody secretion was not only unhelpful but counterproductive to the antitumor response. Analysis of MC38 tumor-draining LNs of IgMi mice on DPI 7 revealed a higher percentage of GCB cells (Fig. 1b), a lower percentage of plasmablasts (Fig. 1c), and that the extent of GCB expansion correlated strongly to reduced tumor size (Supplementary Fig. 1d), encouraging us to study whether accumulating activated B cells contributed to anti-tumor immunity or whether antibodies were somehow inhibitory. Since all constant regions at the *Igh* locus except for IgM (termed Cμ) are deleted in the IgMi mouse model[30], we wished to verify these results in a distinct model lacking plasma cell differentiation and antibody secretion. Accordingly, we studied *Prdm1*$^{fl/fl}$ CD19cre mice that lack Blimp-1 expression specifically in B cells.

Growth of MC38, B16F10 (melanoma), and LLC1 (Lewis lung carcinoma) tumors in *Prdm1*$^{fl/fl}$ CD19cre mice was slower than in *Prdm1*$^{fl/fl}$ mice (Fig. 1d–f and Supplementary Fig. 1f, g). Lack of one copy of CD19 expression in *Prdm1*$^{w/w}$ CD19cre mice showed comparable tumor growth with WT mice, ruling out an effect of CD19 gene dosage (Supplementary Fig. 1e). MC38 inoculation significantly increased numbers of PC and GCB in the lymph nodes (LNs) of control mice, whereas *Prdm1*$^{fl/fl}$ CD19cre mice showed no PC formation (as expected) but further enhanced GCB accumulation (Fig. 1g, h and Supplementary Fig. 1h, i), indicating that Blimp-1 deficient B cells had enhanced GCB responses. However, no differences were seen in tumor-infiltrating GCBs (Supplementary Fig. 2a). Higher percentages of Tfh cells were found in draining LNs of *Prdm1*$^{fl/fl}$ CD19cre mice at 7- and 27-days post-inoculation (DPI) (Supplementary Fig. 2b, c). On DPI 7, *Prdm1*$^{fl/fl}$ CD19cre tumor-infiltrating lymphocytes (TILs) exhibited higher frequencies of IFNγ + CD8 and CD4 T cells (Fig. 1i, j) and GzmB+ CD8 T cells (Supplementary Fig. 2f), and effector memory CD8 and CD4 T cell numbers were significantly increased (Supplementary Fig. 2d, e). While at DPI 27, *Prdm1*$^{fl/fl}$ CD19cre mice and controls had similar numbers of tumor-infiltrating IFNγ+ and GzmB+ CD8 T cells (Supplementary Fig. 2g, h), in *Prdm1*$^{fl/fl}$ CD19cre mice, the frequency of "exhausted" Tim-3 + PD-1 + CD8 T cells in TILs was significantly diminished and the frequency of IFNγ + CD4 T cells was significantly increased (Fig. 1k, l). Treg cell counts in TILs were similar (Supplementary Fig. 2i). These results indicated that prevention of PC differentiation and antibody secretion promoted B cell activation and effector T cell-mediated antitumor immunity.

We tested whether secreted products of MC38 tumor-bearing mice inhibited the anti-tumor response, comparing serum or isolated Ig (Fig. 2a). The Ig fractions, isolated using the IgG + Capto L method, included a range of immunoglobulin classes (Fig. 2b). The fractions tested were either transferred to tumor-bearing mice directly (Fig. 2c) or after heat inactivation (HI) (Fig. 2d). We failed to detect any negative influence of tumor-induced antibodies or PC secreted products on the antitumor response, as serum of MC38 tumor-bearing mice or its isolated immunoglobulin fraction had no effect when transferred into *Prdm1*$^{fl/fl}$ CD19cre mice (Fig. 2a–d). The results suggested that enhanced numbers or function of activated B cells, rather than loss of tumor-promoting secretions, contributed to anti-tumor immunity in both *Prdm1*$^{fl/fl}$ CD19cre and IgMi mice.

scRNA-seq analysis of tumor-infiltrating B cells

To explore the dynamics of tumor-infiltrating B cells, we generated single-cell 5′ RNA and B cell V(D)J libraries using a combination of sorted CD138+ and B220+ B cells from TILs that were isolated from inoculated MC38 tumors on DPI 18. Two datasets from *Prdm1*$^{fl/fl}$ CD19cre (Blimp-1 BcKO) and *Prdm1*$^{fl/fl}$ (Ctrl) mice were merged into an aligned object (Supplementary Fig. 3a). Our analysis revealed 12 cell clusters in total, due in part to the fact that B220 expression is not restricted to B cells, these clusters included 5 NK-related populations, 4 myeloid lineage subsets, T cells, B cells and PC (Supplementary Fig. 3b). The identity of clusters was verified by the expression of canonical cell-type markers that were conserved across genetic deficiency of *Prdm1* in B cells (Supplementary Fig. 3c). We performed an integrative alignment of B and PC, revealing a unique cluster 2 in Blimp-1-deficient B cells after re-clustering (Fig. 3a–c). Feature plots showed that the naive B cell-associated genes *Ccr7* and *Ighd* were in clusters 0, 1, and 5, and *Ighm* was enriched in clusters 1 and 2. In contrast, *Mzb1*, which is upregulated during plasma cell differentiation, was located in clusters 2, 3, and 4 (Fig. 3d). These data indicate that each subcluster of TIL-Bs represents a different developmental stage. Cells in cluster 4 highly expressed plasma cell-related genes *Jchain*, *Derl3,* and *Sdc1*, and so were the terminal destination of B cells, while the signature features in the other clusters exhibited partial similarities but differences in functional potentials (Fig. 3e, f and Supplementary

https://doi.org/10.1038/s41467-025-59622-4

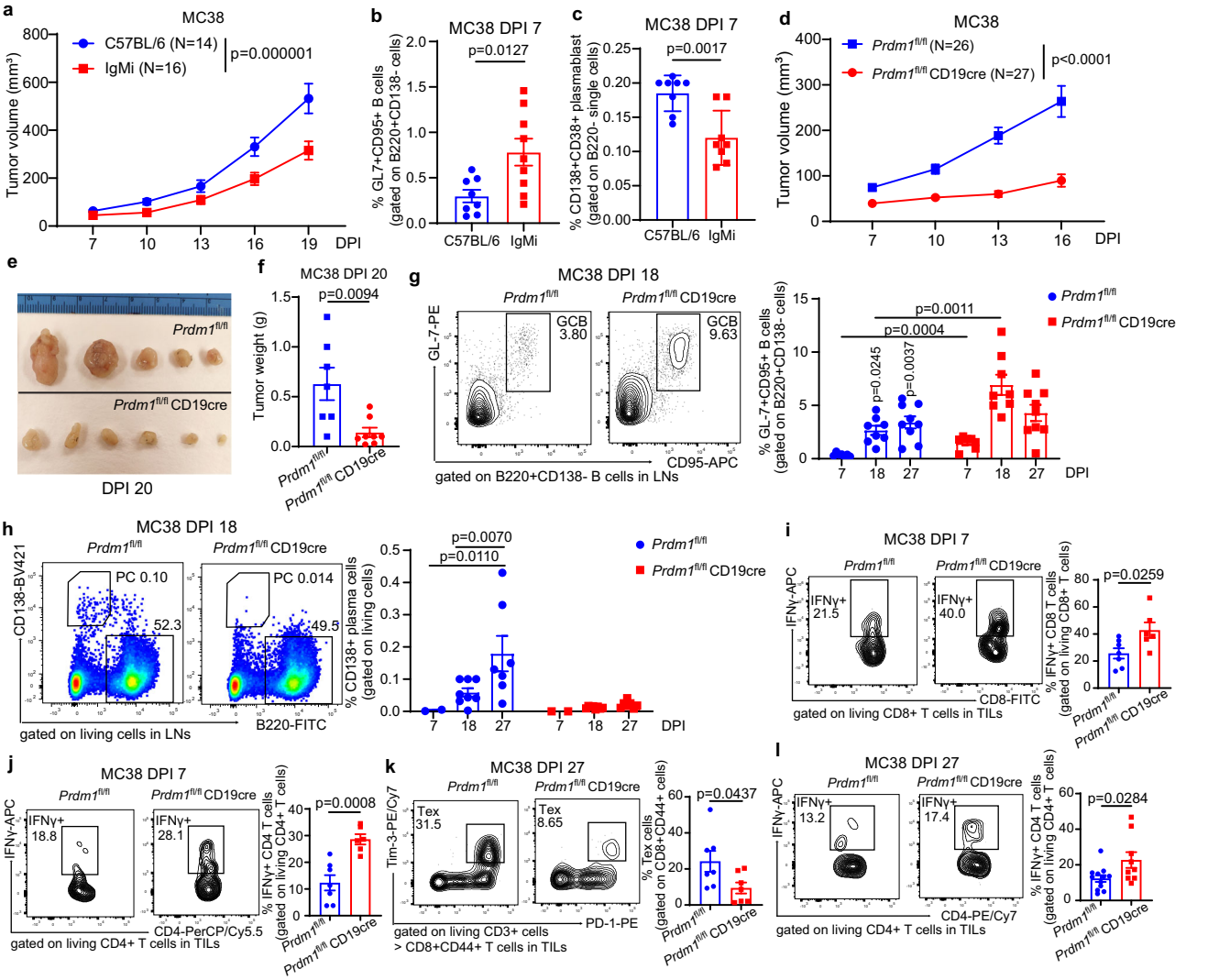

Fig. 1 | Genetic inhibition of plasma cell differentiation has an antitumor effect. **a** Tumor growth in IgMi mice. IgMi or C57BL/6 mice were s.c. implanted with 1×10^6 MC38 tumor cells per mouse. Tumor growth curves were pooled from 2 independent experiments. **b**, **c** Shown are frequencies of GC B cells (**b**) in IgMi ($N = 9$) vs C57BL/6 ($N = 8$) mice and frequencies of plasmablast (**c**) in IgMi ($N = 8$) vs C57BL/6 ($N = 8$) mice in draining LNs on day 7 post-inoculation of MC38 tumor cells. **d** Analysis of tumor growth in *Prdm1*$^{fl/fl}$ ($N = 26$) and *Prdm1*$^{fl/fl}$ CD19cre mice ($N = 30$) implanted s.c. with 1×10^6 MC38 tumor cells per mouse. Data were pooled from 5 independent experiments. **e**, **f** Tumor sizes and weights on day 20 post-inoculation (DPI 20). In (**f**) $N = 7$ for *Prdm1*$^{fl/fl}$ and 8 for *Prdm1*$^{fl/fl}$ CD19cre groups. **g**, **h** Representative flow cytometry plots and frequencies of GC B cells ((**g**); respective numbers of mice analyzed for *Prdm1*$^{fl/fl}$ vs *Prdm1*$^{fl/fl}$ CD19cre groups were as follows: D7: 7 vs 7, D18: 8 vs 8, D27: 9 vs 9) or plasma cells ((**h**); respective numbers of mice analyzed for *Prdm1*$^{fl/fl}$ vs *Prdm1*$^{fl/fl}$ CD19cre groups were as follows: D7: 2 vs 2, D18: 8 vs 8, D27: 7 vs 7) in LNs on day 7, 18, 27 post inoculation of MC38 tumor cells. **i**, **j** Representative flow cytometry plots and frequency of tumor-infiltrating IFNγ + CD8 T cells (**i**) or IFNγ + CD4 T cells (**j**) from *Prdm1*$^{fl/fl}$ ($N = 7$) vs *Prdm1*$^{fl/fl}$ CD19cre mice ($N = 6$) on DPI 7. **k**, **l** Representative flow cytometry plots and frequency of tumor-infiltrating exhausted CD8 T cells ((**k**); *Prdm1*$^{fl/fl}$ ($N = 7$) vs *Prdm1*$^{fl/fl}$ CD19cre mice ($N = 7$)) or IFNγ + CD4 T cells ((**l**); *Prdm1*$^{fl/fl}$ ($N = 12$) vs *Prdm1*$^{fl/fl}$ CD19cre mice ($N = 9$)) on DPI 27. Flow cytometry data (**b**, **c** and **g**–**l**) were from at least 3 independent experiments. Each point in graphs (**b**, **c**, **f**–**l**) represents the value obtained in an independent mouse. Bars are presented as mean ± SEM. *P* values were calculated with the two-tailed unpaired *t*-test (**b**, **c**, **f**, **g** and **i**–**l**), Two-way ANOVA (**a**, **d**, **g** and **h**) and exact *p* value shown in figures. Source data are provided as a Source Data file.

Data 1). B cells in clusters 0 and 1 had many similar gene profiles. They were presumed to be in the priming state because of the high expression of cell proliferation-related genes, such as ribosomal proteins (RPs) genes[31]. B cells in clusters 2 and 3 had consistent upregulation of *Apoe*, which mediates B cell antigen uptake[32]; they also consistently upregulated *Fcrl5* and *Fcgr2b*, which modulate BCR signaling[33,34]. Among potential cell surface markers that discriminate cluster 2, we noted enhanced expression of *Cd9* and *Ptprj* (CD148) (Fig. 3f), which we exploited in subsequent experiments (see below). B cells in cluster 3 expressed the markers of Age-associated B cells (ABCs), such as *Tbx21*, *Ighg2*, *Cxcr3*, and *Cd86*, referring to their antigen-presenting function[35,36]. However, compared with upregulated features in cluster 3, cluster 2 had broader and higher expression of *S100a6*, *Ighm*, and *Cyp4f18*. We obtained a pseudotime trajectory suggesting cluster 2 and 3 represent a transitional state, while cluster 2 points to a non-PC endpoint (Supplementary Fig. 4a). Activated B cells in clusters 0, 1, and 5 had more dark zone (DZ) gene expression, clusters 3 and 4 enriched clear light zone (LZ) characteristics and cluster 2 was more likely in the LZ distribution but the cells in cluster 2 also expressed typical DZ genes such as *Bcl6*, *Son*, *Tcf7*, and *Pax5* (Supplementary Fig. 4c)[37,38]. Biological process (BP) of gene ontology (GO) analysis of the differentially upregulated expression indicated that, except for cluster 5, the rest of the clusters were in the processes of B cell activation, proliferation and differentiation, and B cells in clusters 0, 2, and 3 were predicted to have the abilities of antigen processing and presentation (Supplementary Fig. 4b). Enriched GO

https://doi.org/10.1038/s41467-025-59622-4

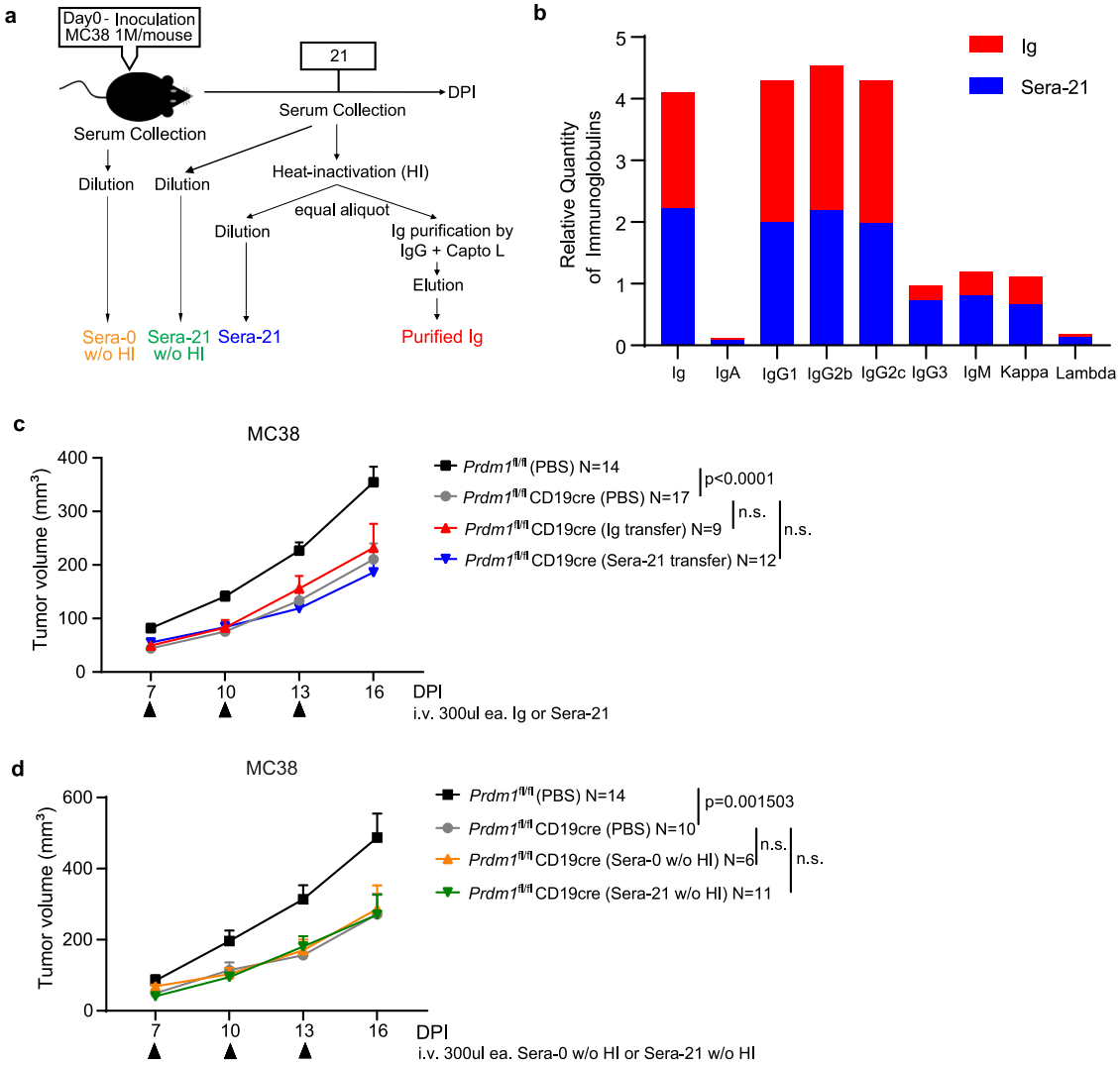

Fig. 2 | Antibodies appear to be dispensable in controlling tumor growth. **a** Experimental outline for serum and immunoglobulin (Ig) preparations. **b** Comparable immunoglobulin components in Ig and serum samples. **c** Failure of Ig or serum from WT tumor-bearing mice to reverse tumor control in *Prdm1*$^{fl/fl}$ CD19cre mice. *Prdm1*$^{fl/fl}$ and *Prdm1*$^{fl/fl}$ CD19cre mice were implanted s.c. with 1×10^6 MC38 tumor cells per mouse on day 0. Sera-21 refers to a pool of sera collected from MC38-bearing mice on day 21 post-inoculation. Ig was purified from Sera-21 using a mixture of protein G and Capto L beads. Each mouse in the Ig and Sera-21 transfer groups received 0.3 ml of Ig or Sera-21 dilutions i.v., respectively, on days 7, 10, and 13 (indicated with black arrows). Data were pooled from 4 independent experiments. **d** *Prdm1*$^{fl/fl}$ and *Prdm1*$^{fl/fl}$ CD19cre mice were implanted s.c. with 1×10^6 MC38 tumor cells per mouse. Sera-0 without heat-inactivation (w/o HI) were collected from C57BL/6 mice without tumor burden. Sera-21 without heat-inactivation (w/o HI) were collected on day 21 after MC38 inoculation. Each mouse in the transfer groups received 0.3 ml i.v. of Sera-0 (w/o HI) or Sera-21 (w/o HI) dilutions, respectively, on days 7, 10, 13 (indicated with black arrows). Data were pooled from 4 independent experiments. Bars show mean ± SEM. *P* values were calculated with two-tailed unpaired multiple *t*-tests with Holm–Sidak's correction (**c**, **d**), and n.s. denote $P > 0.05$. Source data are provided as a Source Data file.

analysis of cellular component (CC) and molecular function (MF) showed that B cells in cluster 2 could have more potential in cell deformability and cell-to-cell binding activity (Supplementary Fig. 4d). These results are consistent with a model in which the unique cluster 2 found in *Prdm1*$^{fl/fl}$ CD19cre mice contributes to BCR recognition of tumor-specific antigens under the process of encountering tumor cells.

B cells recognize and present tumor-specific antigens

B cells can either present antigens passively or by specific uptake through the B cell receptor (BCR)[19], which is more efficient, though the frequency of antigen-specific B cells is often low. Presentation to T cells in turn can lead to B cell clonal expansion. When we consolidated VDJ sequencing results to the level of the individual cell barcodes, we found expanded clonotypes specifically in cluster 2 of Blimp-1 BcKO mice (Fig. 4a). There was minimal sequence overlap, as only a single immunoglobulin κ chain (IGKC) variable sequence was shared between Blimp-1 KO and control B cells (Fig. 4b and Supplementary Data 2). Fourteen clonotypes were detected in Blimp-1 KO B cells in total, and only abundant clonotype 6 (AC-6) and AC-7 were non-IgM isotypes among these clonotypes (Fig. 4c). In addition, among the top 4 expanded clonotypes (AC-1 to AC-4) of Blimp-1 KO B cells the extent of somatic hypermutation exceeded 2% while the clonotype detected in the control was barely mutated (Fig. 4d). These results suggested the possibility that the tumor-infiltrating B cells undergoing antigen selection contributed to tumor-specific antigen recognition. The heavy chain of AC-1 from Blimp-1 KO B cells was an IgM isotype encoded by IGHV6-3/IGHJ3, and the light chain by IGKV14-111/IGKJ2. The heavy chain of AC-2, also an IgM isotype, used IGHV1-9/IGHJ2, and the light chain was IGKV5-39/IGKJ2. IgBlast analysis[39] indicated that IGHV of AC-1 and AC-2 were 3.06% and 4.86% somatically mutated at the nucleotide sequence level, respectively, whereas IGKV of AC-1 and AC-2 had

https://doi.org/10.1038/s41467-025-59622-4

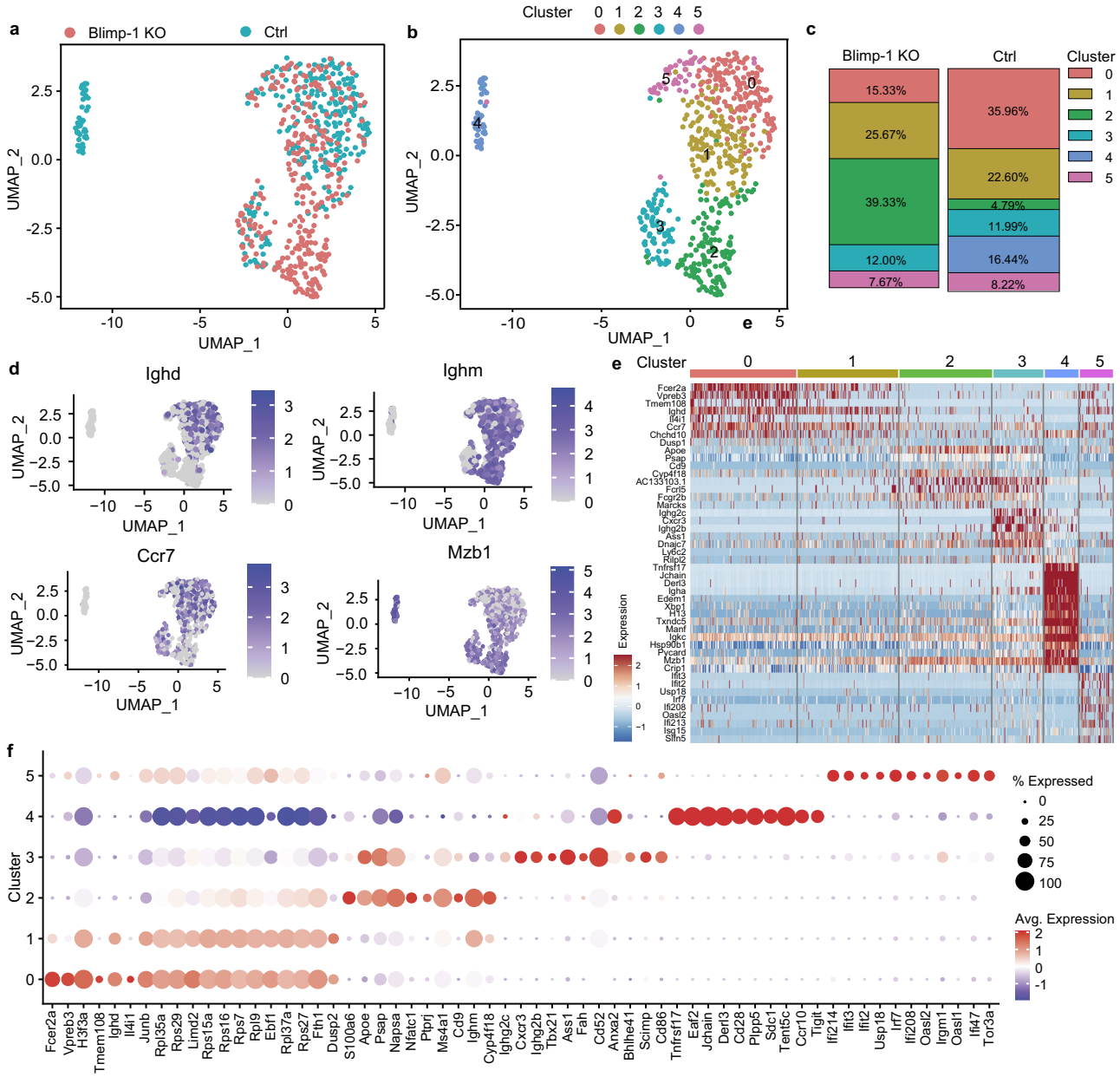

Fig. 3 | Integrated analysis of tumor-infiltrating Blimp-1 knock-out (KO) B cells and control B cells using scRNA-seq technologies. a UMAP plots showing subclusters of tumor-infiltrating B cells (clusters marked with red border in Supplementary Fig. 3c) from B cell-specific Blimp-1 knockout (Blimp-1 BcKO) mice (300 cells) and control (Ctrl) mice (292 cells) after alignment. **b** Distribution of 6 subpopulations across Blimp-1 BcKO and Ctrl group after alignment. **c** The proportions of different B clusters from Blimp1 BcKO and Ctrl groups. **d** Feature plots showing the distribution of expression of the indicated molecules in B-cell subclusters. A total of 592 cells were projected onto a UMAP plot. **e** Heatmap summarizing the differential gene expression in each subcluster. **f** Dot plots showing upregulated genes for each cluster. Dot size reflects the percentage of cells in a cluster expressing the gene, dot colors indicate average expression levels. Source data are available in the Gene Expression Omnibus (GEO) under accession number GSE289410.

1.08% and 0.72% somatic mutations, respectively (Supplementary Fig. 4e). We found that Serine (S) and Threonine (T) were used more than other amino acids in the junctions of AC-1 to AC-4, and there was a similar usage pattern of S and T within the junctions (Fig. 4e). To assess possible specificity, we expressed AC-1 and AC-2 as chimeric human IgG1 antibodies and tested their ability to bind tumor cells. Surface staining confirmed that AC-1 and AC-2 were able to interact with cognate MC38 tumor cells, although high antibody concentrations were required, and that AC-1 could unexpectedly cross-react to LLC1 tumor cells (Fig. 4f, g). Under identical staining conditions, neither AC-1 nor AC-2 was able to interact with B16F10, spleen cells or mouse primary colonic epithelial cells (Fig. 4h–j). These data confirmed that these expanded clones of TIL-B were reactive to cognate tumor cells and presumably could promote antigen presentation.

To further assess the role of tumor antigen-specific B cells in antitumor immunity, we took advantage of MD4 BCR transgenic mice in which ~90% of B cells carry a defined antigen receptor reactive to hen egg lysozyme (HEL), in which the endogenous BCR repertoire is consequently limited[40,41]. The tumor growth of B16F10 (Fig. 5a, b) and MC38 (Fig. 5c, d) in MD4 mice was faster than that in control mice. We then generated a stable cell line of B16F10 expressing membrane-bound HEL (termed B16F10-mHEL) and verified by flow cytometry the surface expression of mHEL (Fig. 5e). We found that growth of B16F10-mHEL in MD4 mice was now slower than in control mice (Fig. 5f, g).

https://doi.org/10.1038/s41467-025-59622-4

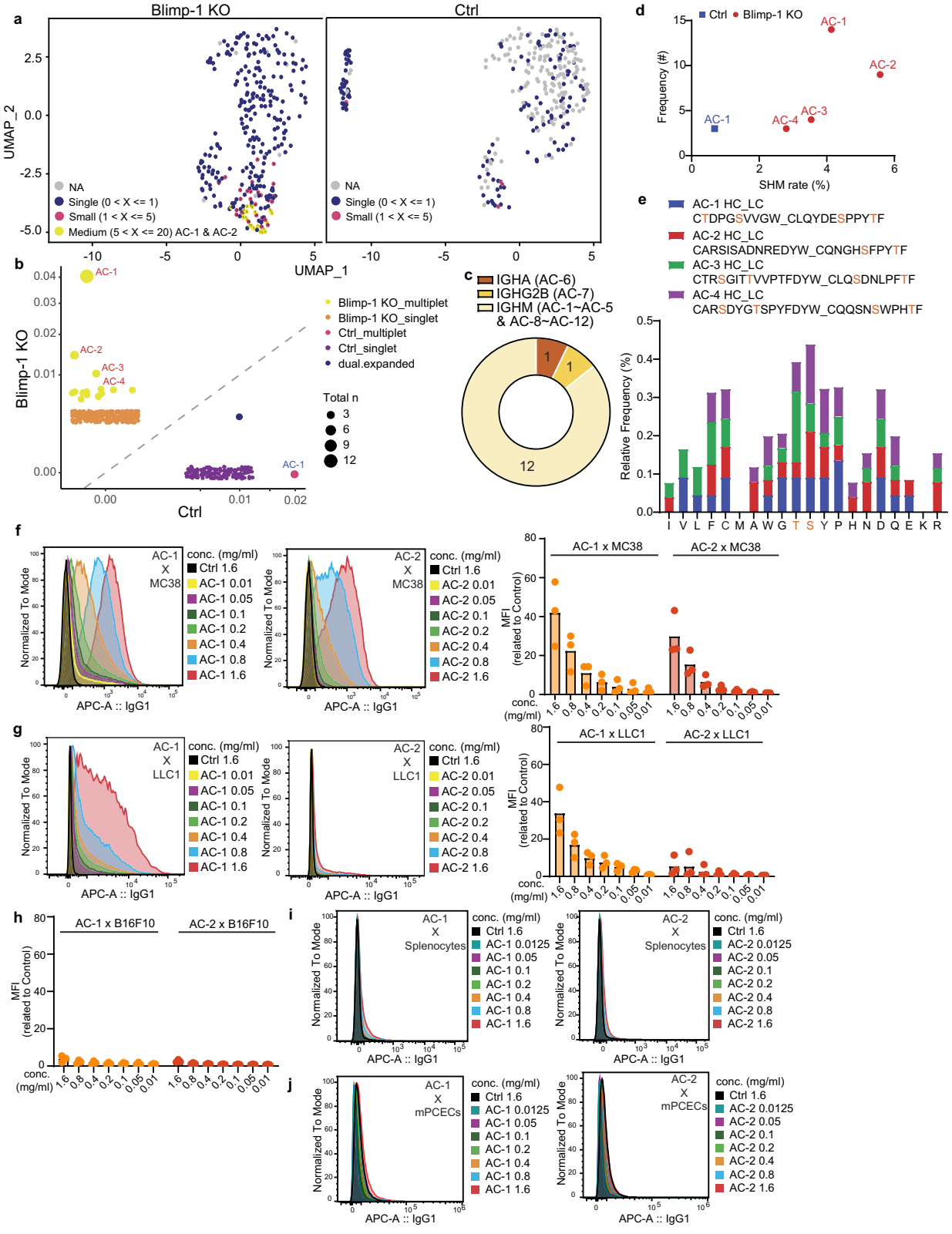

MD4 mice challenged with cognate B16F10-mHEL cells had a higher frequency and absolute number of GC B cells than MD4 mice inoculated with control B16F10 cells (Fig. 5h). More CD86 + MHC-II + B cells and CD80 + MHC-II+ cells were detected in the draining LNs when MD4 mice carried B16F10-mHEL tumors (Fig. 5i, j). Compared to MD4 mice bearing B16F10-Ctrl cells, MD4 mice inoculated with B16F10-mHEL had a higher proportion of tumor-infiltrating CD80 + MHC-II + B cells and CD86 + MHC-II + B cells, as well as increased expression of CD80 and CD86 on B cells (Fig. 5k, l). Though the proportion of PCs in draining LNs showed no difference between MD4 mice receiving B16F10-mHEL or B16F10-Ctrl tumor cells, the absolute number of PC was higher in MD4 mice inoculated with tumor cells expressing mHEL, suggesting the tumor-induced antibodies or PC accumulation was driven by cell expansion in draining LNs (Fig. 5m). Consistent with an antigen-

Fig. 4 | Clonotypes identified from Blimp-1 KO B cells can target cognate tumor cells. a UMAP projection showing expanded clonotypes enriched in a unique cluster that was generated by Blimp-1 deficiency. Plots were split by genotype (300 cells in Blimp-1 BcKO group and 292 cells in control group), with larger clone sizes indicated in yellow. Clonotype serial numbers are shown on their dots. **b** Scatter plots allowing for the proportion of clonotypes between Blimp-1 KO and Control (Ctrl) B cells. Dots are sized for clonotype frequencies. **c** Heavy chain class distribution of 14 abundant clonotypes (AC) resulting from Blimp-1 deficiency. Except for AC-6 and AC-7, the remaining clonotypes (AC-1 to AC-5, AC-8 to AC-12) were IgM isotype-clones. **d** Correlation between percent somatic hypermutation (SHM) and clonotype frequency. Dots are only shown if clonal members exceed 3. **e** The proportion of amino acid usage in CDR3 junctions of 4 clonal expansions in Blimp-1 KO B cells. HC heavy chain, LC light chain. **f** Representative histograms of median fluorescence intensity (MFI) obtained from titrated concentrations of AC-1 (left) and AC-2 (right) bound to the surface of MC38 tumor cells. **g** AC-1 but not AC-2 can cross-react to the surface of LLC1 tumor cells. MFI of titrated concentrations of AC-1 (left) and AC-2 (right). **h**–**j** MFI obtained from titrated concentrations of AC-1 (left) and AC-2 (right) showed minimal ability to bind to the surface of B16F10 cells (**h**), splenocytes (**i**) or mouse primary colonic epithelial cells (mPCECs) (**j**). Each point in the graphs (**f**, **g** and **h**) represents the value of one sample from each experiment and pooled data from 3 independent experiments. Source data are provided as a Source Data file.

specific reaction, more anti-HEL antibodies were detected in the sera of MD4 mice receiving B16F10-mHEL tumor inoculation than in the sera of MD4 mice inoculated with B16F10-Ctrl tumors (Fig. 5n). To evaluate the tumor-specific antibody efficacy in this model, we immunized the MD4 mice with a mixture of HEL and LPS to obtain serum containing IgM anti-HEL antibodies (termed sera-HEL). We introduced sera-HEL to the control mice inoculated with B16F10-mHEL tumor cells and the transferred serum seemed to slow down the tumor growth on D10 but eventually could not suppress the tumor mass enlargement (Supplementary Fig. 7f). These data indicate that tumor-specific antigen recognition and presentation by B cells facilitated antitumor immunity. Taken together with the results described above, the data support a model in which a block in plasma cell differentiation facilitates, rather than hinders, tumor recognition by favoring antigen-specific recognition and presentation by B cells to T cells, a process that normally precedes, and is terminated by, plasma cell differentiation.

MHC II requirement and elevated expression of costimulatory molecules contribute to antitumor immunity by B cells

We investigated the role of antigen presentation in the antitumor response of *Prdm1*$^{fl/fl}$ CD19cre mice. An anti-MHC II antibody used to block antigen presentation to CD4 T cells in vivo completely abolished the effect of Blimp-1-deficiency in B cells, as tumor growth became comparable in anti-MHC II antibody-treated *Prdm1*$^{fl/fl}$ CD19cre and control mice, and similar to that in untreated control mice (Fig. 6a). Tumor challenge of *H2-Ab1*$^{fl/fl}$ Mb1cre mice lacking MHC II specifically in B cells confirmed that both MC38 and B16F10 tumors grew significantly faster even in these Blimp1-sufficient mice when recipient B cells lacked MHC II expression (Supplementary Fig. 5a, b). We conclude that the enhanced antitumor response of *Prdm1*$^{fl/fl}$ CD19cre mice, as well as the more modest repression of plasma cell-sufficient mice, depends on antigen presentation by B cells to CD4 T cells.

We further compared *Prdm1*$^{fl/fl}$ CD19cre and control B cells in tumor-bearing WT or KO mice. Although DPI 7 TILs had similar percentages of CD80+ and CD86 + B cells (Supplementary Fig. 5c), draining LNs of *Prdm1*$^{fl/fl}$ CD19cre mice had more CD80 + B cells and a higher B cell expression of CD80 (Fig. 6b, c and Supplementary Fig. 5e), while CD86 + B cell numbers were unchanged (Supplementary Fig. 5d). By DPI 27, TILs of *Prdm1*$^{fl/fl}$ CD19cre mice had a significantly higher frequency of both CD80+ and CD86 + B cells and higher levels on B cells of both CD80 and CD86 (Fig. 6d–g). CD80 and CD86 expressed on antigen-presenting cells are essential for T cell activation and proliferation by engaging CD28[42]. Thus, Blimp-1-deficient B cells likely have enhanced costimulatory function contributing to an elevated antitumor T cell response.

Our data suggest that B cells that are activated by tumor antigens persist longer in a transitional activated or germinal center stage when their plasma cell differentiation is blocked, which generates a repertoire-selected population characterized by high levels of CD80 and CD86 costimulatory molecules that are predicted to efficiently present tumor antigens to T cells via the MHC II pathway, leading to enhanced antitumor immunity.

To explore the mechanism for increased levels of costimulatory factors on Blimp-1-deficient B cells, we analyzed IgMi mice with intact Blimp-1 expression. Compared with *Prdm1*$^{fl/fl}$ CD19cre mice, IgMi mice showed similar changes in lymphoid activation within MC38 tumors or in draining LNs (Supplementary Fig. 6a–k), except that they lacked an increased frequency of CD86 + B cells in TILs on DPI 27 (Supplementary Fig. 6l), suggesting that CD80 expression on B cells may be critical to excite cytotoxic T cell responses, and that class switch recombination may not influence antigen presentation on activated B cells in this experimental model. Assessing the commonalities between Blimp-1 BcKO and IgMi models, it appears that blocking plasma cell differentiation either way led to accumulation of activated B cells, including GCBs, which have enhanced antigen presentation capability compared to PCs.

Inhibition of plasma cell differentiation diverts B cells to a memory-like cell surface phenotype

To investigate the fate of B cells when their path to PC was blocked, we first took advantage of CD9 (encoded by *Cd9*) and CD148 (encoded by *Ptprj*), which identify the C2 population that is enriched in *Prdm1*$^{fl/fl}$ CD19cre mice (Fig. 7a). Then we confirmed that among tumor-infiltrating B cells in *Prdm1*$^{fl/fl}$ CD19cre mice, CD9 + CD148 + B cells made up a significantly higher proportion than they did in *Prdm1*$^{fl/fl}$ mice (Fig. 7b). When we compared the distinct features of CD9 + CD148 + B cells compared to CD9−CD148− B cells in Blimp-1 deficient condition, we found that CD9 + CD148 + B cells had higher levels of CD20 (encoded by *Ms4a1*), CD73, PD-L2, IgM, and CD80, and lower levels of IgD (Fig. 7c). CD80, PD-L2, and CD73 identify memory B cells[43]. In addition, more CD9 + CD148 + B cells were detected in draining LNs of *Prdm1*$^{fl/fl}$ CD19cre mice compared to their control mice (Fig. 7d). CD73 and PDL2 was higher on CD9 + CD148 + B cells in tumors as well as in draining LNs compared to CD9−CD148− B cells in the same tissues, however significantly higher CD80 expression was only seen on CD9 + CD148 + B cells in draining LNs of *Prdm1*$^{fl/fl}$ CD19cre mice (Fig. 7e). The increased numbers of CD9 + CD148 + B cells in both draining LNs and among tumor-infiltrating CD9 + CD148 + B cells detected on DPI 7 in *Prdm1*$^{fl/fl}$ CD19cre mice suggested the expansion of this B cell population occurred simultaneously with the GC response (Fig. 7f). The phenotype of increased numbers of CD9 + CD148 + B cells in draining LNs and higher frequencies of tumor-infiltrating CD9 + CD148 + B cells was observed clearly in IgMi mice as well (Supplementary Fig. 6m–o), again suggesting that the expansion of these memory-like B cells is not solely dependent on the loss of Blimp-1 expression but is associated with PC blockade.

These data indicate that when the branch of differentiation to PC was inhibited, activated B cells not only increased tumor-specific antigen presentation by BCR selection but also generated a memory-like B cell population with high expression of CD9 and CD148. The CD9 + CD148 + B cell population may eventually be retained in adjacent LNs while maintaining memory B cell features, including expression of CD73, PDL2, and CD80. Most importantly, although the CD9 + CD148+ memory-like B cells are present at low frequency in mouse tumor samples, they are detectable in normal conditions that

https://doi.org/10.1038/s41467-025-59622-4

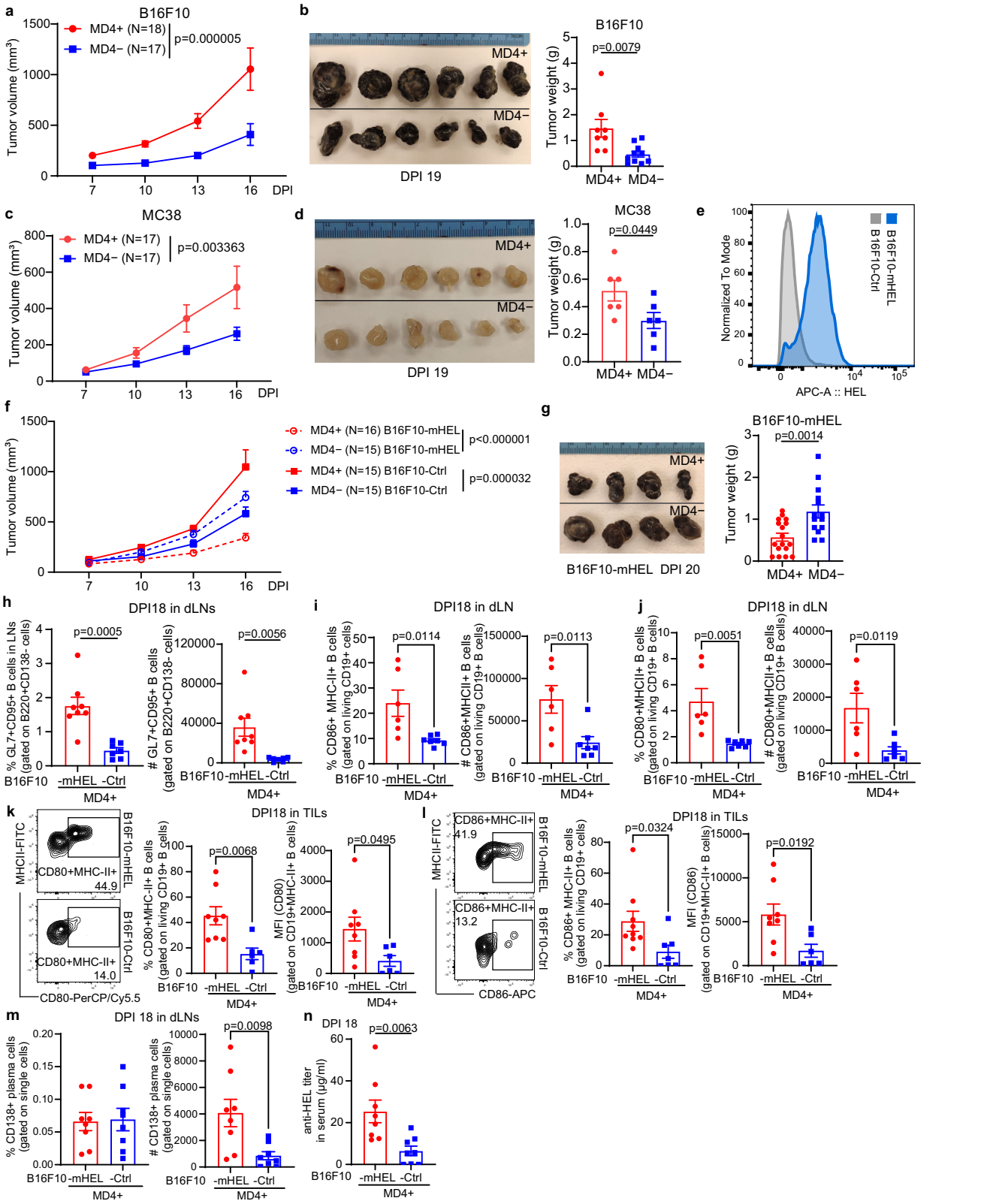

provide the possibility to participate in local affinity selection and antigen presentation.

VPA, a Blimp-1 inhibitor, can be used for tumor treatment

We then explored the possibility of treating cancer by targeting Blimp-1. A previous study reported that valproic acid (VPA) sodium salt dissolved in the drinking water silenced Blimp-1 expression by promoting the degradation of *Prdm1* mRNA[44]. Accordingly, we inoculated MC38 into C57BL/6 mice on day 0, at which time we substituted drinking water containing VPA. Remarkably, we found that both 0.4% and 0.8% VPA in drinking water suppressed tumor growth (Fig. 8a, b), with a stronger effect for 0.8% VPA. Consistent with the presumed mechanism of action, plasma cell generation was repressed, while GCBs accumulated in LNs of mice treated with VPA (Fig. 8c, d). Compared to the

https://doi.org/10.1038/s41467-025-59622-4

Fig. 5 | BCR recognition of tumor-specific antigens promotes antitumor immunity. a, **b** Analysis of tumor growth in MD4+ ($N = 18$) and non-transgeneic MD4− ($N = 17$) littermate mice implanted s.c. with 1×10^6 B16F10 tumor cells per mouse. Data were pooled from 2 independent experiments. **b** Tumor sizes (left) and weights (right) on DPI 19. **c**, **d** Accelerated growth of MC38 tumors in MD4 mice. MD4+ ($N = 17$) and MD4− ($N = 17$) mice were implanted s.c. with 1×10^6 MC38 tumor cells per mouse. Data were pooled from 2 independent experiments. **d** Tumor sizes (left) and weights (right) on DPI 19. **e** Histogram comparison of membrane-bound HEL (mHEL) expression in B16F10-mHEL and control B16F10 cells. **f**, **g** Analysis of tumor growth in MD4+ and MD4− mice implanted s.c. with 1×10^6 control B16F10 cells (B16F10-Ctrl) or with B16F10 cells stably expressing membrane-bound HEL (B16F10-mHEL). Data were pooled from 5 independent experiments. **g** Tumor sizes (left) and weights (right) on DPI 20. **h** Representative flow cytometry plots, number and frequency of GC B cells in draining LNs of MD4+ mice implanted with B16F10-mHEL or B16F10-Ctrl cells on DPI 18. **i**, **j** Frequency and number of activated CD86 + MHC-II + B cells (**i**) and CD80 + MHC-II + B cells (**j**) in draining LNs on DPI 18. **k** Representative flow cytometry plots and frequency of tumor-infiltrating CD80 + MHC-II + B cells, and CD80 expression on CD19 + MHC-II + B cells on DPI 18. **l** Representative flow cytometry plots and frequency of tumor-infiltrating CD86 + MHC-II + B cells, and CD86 expression on CD19 + MHC-II + B cells on DPI 18. **m** Proportion and number of plasma cells in draining LNs on DPI 18. **n** ELISA measurement of anti-HEL antibody in serum of MD4+ mice on DPI 18 of B16F10-mHEL or B16F10-Ctrl tumor cells. Each point in graphs (**b**, **d**, **g**, **h**–**n**) represents value obtained in an individual mouse. Flow cytometry and ELISA data were pooled from 3 independent experiments. Bars show mean ± SEM. *P* values were calculated with two-tailed unpaired *t*-test (**b**, **d**, **g**, **h**–**n**), two-tailed unpaired multiple *t*-tests with Holm–Sidak's correction (**a**, **c**, **f**) and exact *p* value shown. Source data are provided as a Source Data file.

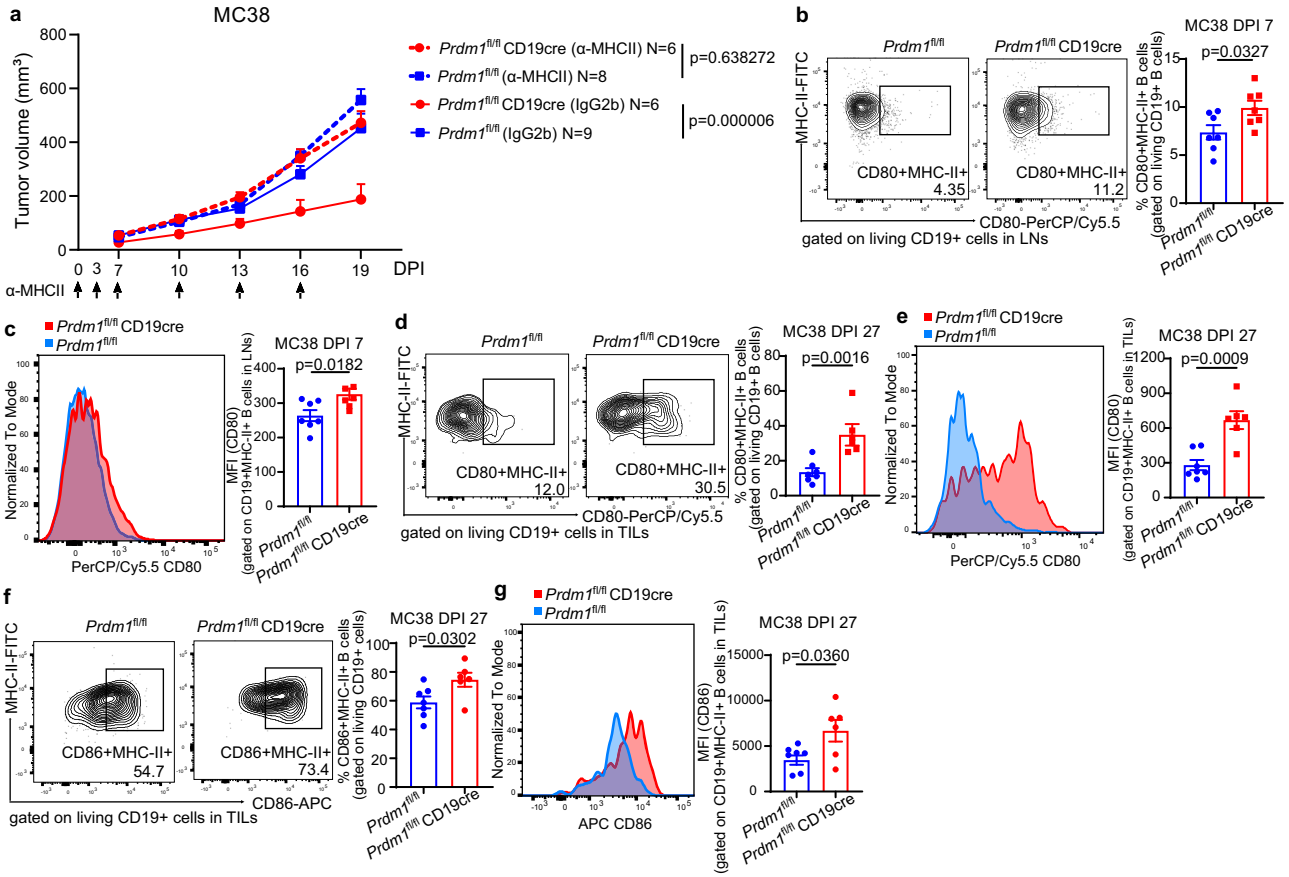

Fig. 6 | Improved tumor control by Blimp-1-deficient B cells requires MHC-II and correlates with elevated expression of costimulatory molecules. a Effect of anti-MHC-II blockade on MC38 tumor growth was assessed by treating *Prdm1*$^{fl/fl}$ and *Prdm1*$^{fl/fl}$ CD19cre mice with anti-MHC-II antibody or IgG2b control on days 0, 3, 7, 10, 13, 16 post inoculation (the days of injection indicated with black arrows); data were pooled from 2 independent experiments. **b** Representative flow cytometry plots and frequency of CD80 + MHC-II + B cells in draining LNs of *Prdm1*$^{fl/fl}$ ($N = 7$) vs *Prdm1*$^{fl/fl}$ CD19cre ($N = 7$) mice on DPI 7. **c** CD80 expression on CD19 + MHC-II + B cells in draining LNs on DPI 7. **d** Frequency of tumor-infiltrating CD80 + MHC-II + B cells in *Prdm1*$^{fl/fl}$ ($N = 7$) vs *Prdm1*$^{fl/fl}$ CD19cre ($N = 6$) mice on DPI 27. **e** CD80 expression on tumor-infiltrating CD19 + MHC-II + B cells on DPI 27. **f** Frequency of tumor-infiltrating CD86 + MHC-II + B cells in *Prdm1*$^{fl/fl}$ ($N = 7$) vs *Prdm1*$^{fl/fl}$ CD19cre ($N = 6$) mice on DPI 27. **g** CD86 expression on tumor-infiltrating CD19 + MHC-II + B cells on DPI 27. Flow cytometry data are from at least 3 independent experiments. Each point in graphs (**b**–**g**) represents an individual mouse. Bars show mean ± SEM. *P* values were calculated with two-tailed unpaired *t*-test (**b**–**g**), two-tailed unpaired multiple *t*-tests with Holm–Sidak's correction (**a**) with exact *p* values shown. Source data are provided as a Source Data file.

control mice, more CD80 + MHC-II+ and CD86 + MHC-II + B cells were detected in draining LNs in the mice treated with VPA (Fig. 8e). Consistent with the phenotypes we found in the Blimp-1 BcKO or IgMi model, in the mice receiving VPA treatment there was a higher proportion of tumor-infiltrating CD80 + MHC-II+, CD86 + MHC-II + B cells and CD9 + CD148 + B cells, significantly increased expression of CD80 or CD86 on B cells within tumors, and more CD9 + CD148 + B cells in draining LNs (Fig. 8f–i). Comparing VPA-treated mice with their controls, though no difference was found in Treg or effector NK cells in tumors, higher frequencies of tumor-infiltrating GzmB+ CD4 T cells and GzmB+ CD8 T cells were observed in the group receiving VPA treatment (Fig. 8j, k). More tumor-infiltrating macrophages were detected in the mice receiving VPA, however, the ratio of CD86+ (M1) to CD206+ (M2) macrophages was comparable between groups (Fig. 8l, m). Importantly,

https://doi.org/10.1038/s41467-025-59622-4

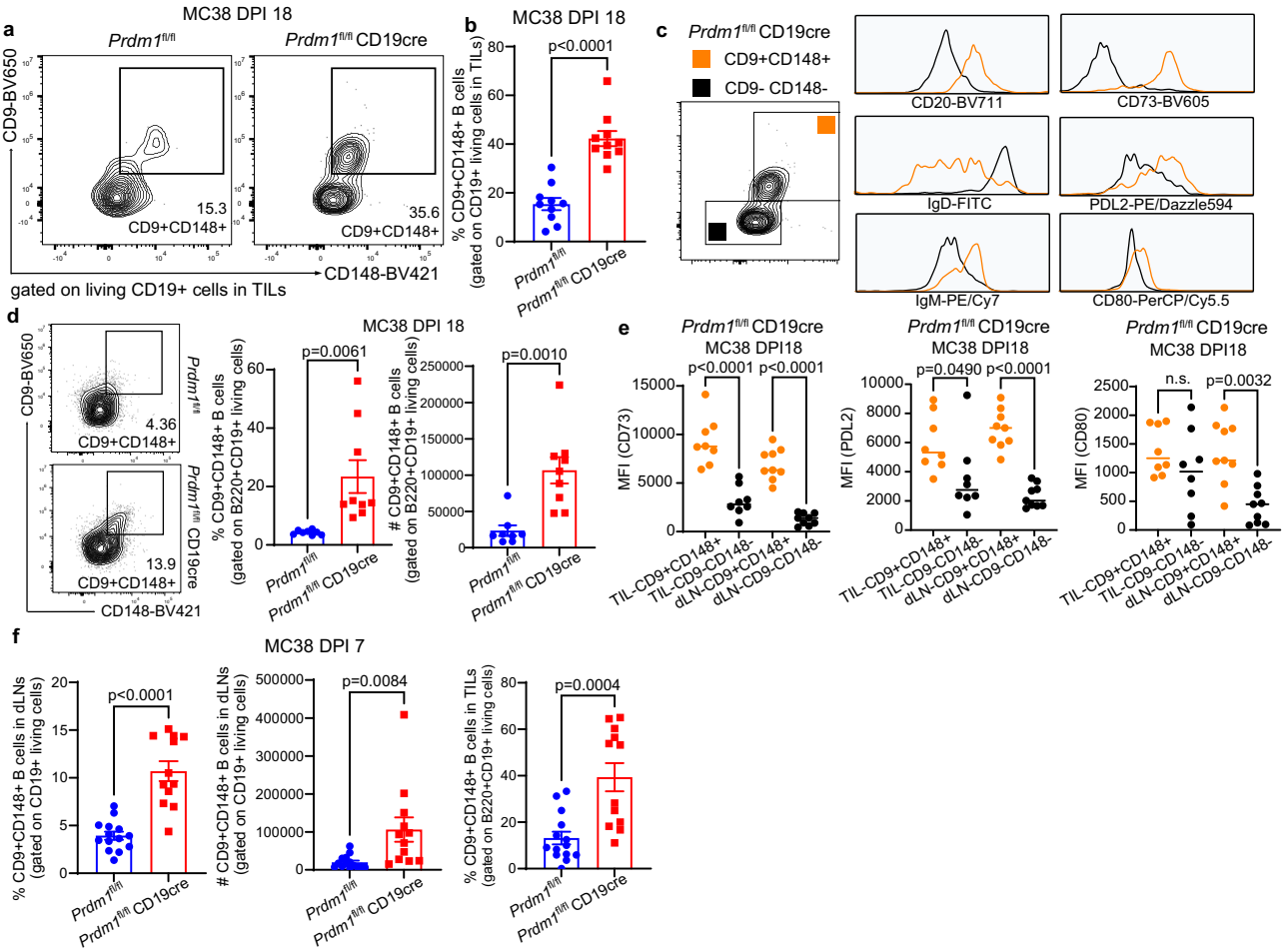

Fig. 7 | Cluster 2-like CD9 + CD148 + B cell population has memory B cell features and is present in smaller numbers in plasma cell-sufficient mice. a On day 18 post-MC38 inoculation, representative flow cytometry plots and frequency of CD9 + CD148 + B cells in tumors. **b** Elevated frequency of CD9 + CD148 + TIL-Bs in *Prdm1*$^{fl/fl}$ CD19cre compared to *Prdm1*$^{fl/fl}$ mice, $N = 10$/group. **c** Analysis of expression of CD20, IgD, IgM, CD73, PD-L2, and CD80 on d18 CD9 + CD148 + TIL-Bs in *Prdm1*$^{fl/fl}$ CD19cre mice. **d** Representative flow cytometry plots and quantification of CD9 + CD148 + B cells of *Prdm1*$^{fl/fl}$ mice ($N = 8$) and *Prdm1*$^{fl/fl}$ CD19cre mice ($N = 9$) in draining LNs on DPI 18. **e** CD73, PDL2 and CD80 expression on tumor-infiltrating or on draining LNs CD9 + CD148 + B cells at DPI 18 in *Prdm1*$^{fl/fl}$ ($N = 8$) vs *Prdm1*$^{fl/fl}$ CD19cre mice ($N = 9$). **f** Frequency and number of CD9 + CD148 + B cells in draining LNs (left and middle) and the proportion of tumor-infiltrating CD9 + CD148 + B cells (right) in *Prdm1*$^{fl/fl}$ ($N = 14$) vs *Prdm1*$^{fl/fl}$ CD19cre mice ($N = 12$) on DPI 7. Flow cytometry data are from 3 independent experiments. Each point in graphs (**b**, **d**–**f**) represents an individual mouse. Bars show mean ± SEM. *P* values were calculated with two-tailed unpaired *t*-test (**b**, **d** and **f**), ordinary one-way ANOVA with Tukey's multiple comparisons test (**e**) with exact *p* value shown, and n.s. denote $P > 0.05$. Source data are provided as a Source Data file.

tumor suppression by VPA failed to occur in both Rag1 KO and J_H/JCkappa double KO mice, indicating that B cells are crucial for the antitumor effect of VPA (Fig. 8n, o). In a more stringent test, VPA treatment for tumor suppression was also effective in a genetically engineered model of spontaneous mammary cancer, MMTV-PyMT mice, where VPA was provided starting at the age of 6 weeks (Fig. 8p). We also took advantage of the VPA therapeutic method combined with the MD4 model to confirm in a high-affinity BCR recognition condition that blocking plasma cell differentiation could increase CD9 + CD148 + B cell expansion in draining LNs or in tumors, enhance effector T cell behavior, and thereby promote stronger tumor growth repression (Supplementary Fig. 7a–e). Therefore, pharmacologic inhibition of Blimp-1 or comparable targeting of B cells may be a viable approach to cancer immunotherapy.

Discussion

The functions of B cells, PC, and antibodies in the natural suppression of cancer have been controversial[45]. In this study, we showed that B cell-specific deletion of Blimp-1, the master regulator of plasma cell differentiation, enhanced antitumor immunity in multiple syngeneic mouse models. IgMi, an independent mouse model with restricted plasma cell differentiation and no class switching, showed similar tumor repression. The enhanced antitumor immunity required B cell recognition of TAAs and antigen presentation via the MHC II pathway and was independent of the antibody secretion function of B cells. In the absence of plasma cell differentiation, B cells exhibited elevated expression of costimulatory molecules CD80 and CD86, while tumor-bearing mice harbored more transitional activated B cells. Therefore, accumulation of activated B cells with costimulatory and tumor-specific antigen-presenting functions led to enhanced antitumor T cell responses and tumor suppression.

The B cell populations that appear to be expanded when PC differentiation is downregulated include GC and memory-like B cells, particularly a unique population characterized by high levels of CD9 and CD148, along with CD73, CD80, PD-L2, and CD20. The latter cells are expanded in draining lymph nodes and among TIL-Bs and include the abundant clones, which have demonstrably undergone proliferation and somatic mutations, presumably related to antigen-specific recognition and interaction with T cells. Our study indicates that the ability of these cells to present to T cells is more important to the

https://doi.org/10.1038/s41467-025-59622-4

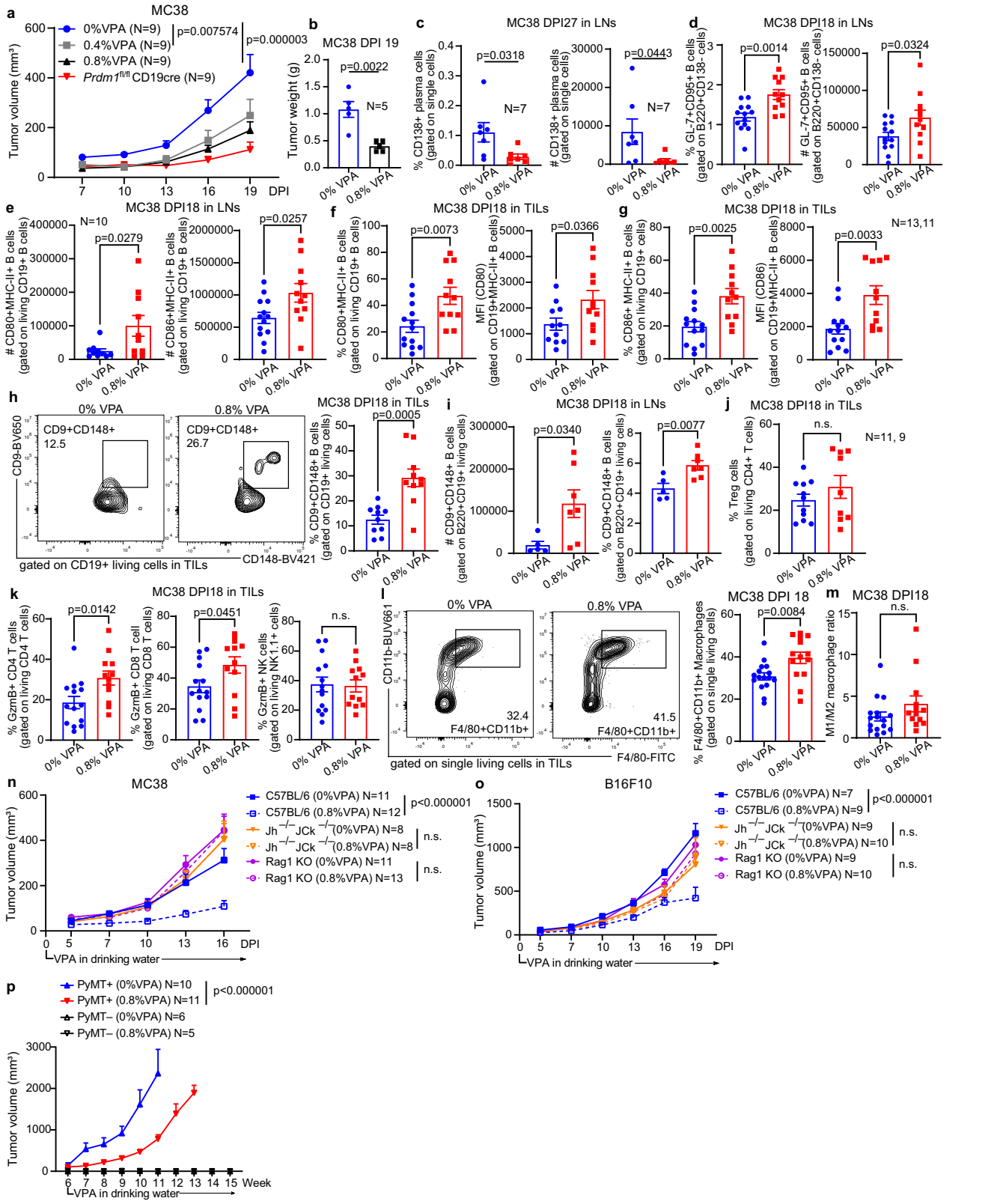

tumor response than their ability to differentiate to antibody secretion.

The contribution of tumor-specific antigen recognition or presentation by B cells is increasingly gaining attention. Some human studies have similarly concluded that TIL-Bs with antigen-presenting function are associated with favorable cancer prognosis[7,46,47]. Recent studies showed that CD20 + B cell-rich TLSs promote immunotherapy responses and survival in sarcoma patients[48]. Among multiple types of carcinoma cases, CD86 + TIL-Bs co-localized in TLS, and more antigen-presenting B cells were observed in TLS-high samples that correlated with better CD8 T cell responses[46]. CD8+ TILs that colocalized with antigen-experienced CD20 + TIL-Bs with high expression of antigen presentation-related markers displayed stronger cytolytic immune responses than CD8+ TILs working alone within tumors[7]. In non-small

Fig. 8 | Blimp-1 inhibitor VPA reduces tumor growth in vivo through a B cell dependent mechanism. a C57BL/6 and *Prdm1*$^{fl/fl}$ CD19cre mice were implanted with MC38 and given drinking water containing 0%, 0.4%, or 0.8% VPA from day 0. **b** Tumor weights. **c** Frequency and number of plasma cells in draining LNs of VPA-treated mice on day 27 post-MC38 inoculation. **d** Proportion and number of GCB in draining LNs on DPI 18, *N* = 13, no VPA; *N* = 11, 0.8% VPA. **e** Number of activated CD80 + MHC-II + B cells (*N* = 10) and CD86 + MHC-II+ (*N* = 13, no VPA; *N* = 11, 0.8% VPA) B cells in draining LNs on DPI 18. **f** On DPI 18, frequency of tumor-infiltrating CD80 + MHC-II + B cells, *N* = 13, no VPA; *N* = 11, 0.8% VPA, and CD80 expression on CD19 + MHC-II + TIL-B cells, *N* = 11/group. **g** Proportion of CD86 + MHC-II + B cells and CD86 level on CD19 + MHC-II + B cells within tumors. **h** Representative flow plots and frequency of CD9 + CD148 + TIL-B cells on DPI 18, *N* = 10. **i** Number and proportion of CD9 + CD148 + B cells in draining LNs on DPI 18, *N* = 5, no VPA; *N* = 7, 0.8% VPA. **j** Percentage of Treg cells within tumors on DPI 18. **k** Proportion of tumor-effector CD4 T cells, CD8 T cells and NK cells on DPI 18, *N* = 14, no VPA; *N* = 12, 0.8% VPA. **l** Representative flow cytometry plots and frequency of tumor-infiltrating CD11b + F4/80+ macrophages on DPI 18, *N* = 11, no VPA; *N* = 9, 0.8% VPA. **m** Ratio of CD86 + M1 macrophages and CD206 + M2 macrophages in tumor on DPI 18, *N* = 16, no VPA; *N* = 14, 0.8% VPA. **n**, **o** Analysis of tumor growth in C57BL/6, Jh$^{-/-}$JCk$^{-/-}$ mice, or *Rag1*$^{-/-}$ mice implanted with MC38 (**n**) or B16F10 (**o**) tumor cells and given 0% or 0.8% VPA from day 0. **p** Spontaneous tumor growth in MMTV-PyMT mice treated with VPA. Water containing 0% or 0.8% VPA was provided starting at age of 6 weeks until experimental endpoints. Data were from 2 independent experiments (**n**, **o**). Flow cytometry data were from 2 to 3 independent experiments, and each dot in graphs (**b**–**m**) represents an individual mouse. Bars show mean ± SEM. *P* values were calculated with the two-tailed unpaired *t*-test (b–**m**), two-tailed unpaired multiple *t*-tests with Holm–Sidak's correction (**a**, **n**–**p**), *p* values shown, n.s. denotes $P > 0.05$.

cell lung cancer patients, activated TIL-Bs (CD19 + CD69 + CD27 + CD21 +) were found to present antigen to CD4+ TILs and promoted their effector function; conversely, exhausted TIL-Bs (CD19 + CD69 + CD27 − CD21−) were associated with a Treg phenotype[47], suggesting tumor-specific antigen presentation by B cells may have heterogeneous outcomes. In another study of muscle-invasive bladder cancer (MIBC) patients, CD19 + TIL-Bs had higher CD80 and CD86 expression than CD19+ peripheral blood B-cells, which contributed to more CD44 expression on CD4+ TILs that was associated with improved survival[49]. Moreover, in doxorubicin-treated MIBC patients, B cells with increased CD86 levels correlated with improved antigen presentation[50]. Taken together, these observations from cancer patients indicate that B cells acting as antigen-presenting cells are important in exerting anti-tumor functions, which is also consistent with our findings in mice, suggesting that promoting B cell antigen presentation may be a powerful way to improve antitumor immunity.

The clonotypes identified within tumors from *Prdm1*$^{fl/fl}$ CD19cre mice bound to the surface of cognate MC38 tumor cells and were among a unique CD9 + CD148+ memory-like B cluster 2 with high clonal expansion. Their apparently low affinity might be selected by peripheral tolerance mechanism to avoid attacking normal tissues[51]. Despite the apparent low affinity of the recombinant IgG forms of AC-1 and AC-2, as BCRs interacting with surface antigens on tumors, they may excel at capturing and presenting low-abundance antigens compared to antigen non-specific myeloid cells. As most TAAs are intracellular and unreachable to effective adoptive cell therapy, such as chimeric antigen receptor T therapy[52], our findings suggest it may be useful to identify weakly expressed, targetable exposed molecules on malignant solid tumors. In summary, the somatically mutated clonotypes targeting cognate tumor cells are likely the major contributors to tumor-specific antigen presentation by B cells in plasma cell deficient mice and their expansion is likely the result of such interactions with CD4 T cells.

It has been reported that IgG+ PC can produce tumor-specific antibodies, which may promote antitumor immunity by driving antibody-dependent cellular cytotoxicity and phagocytosis, complement activation, and enhancing antigen presentation by dendritic cells[1]. In addition, it has also been reported that IgA+ PC exert immunosuppressive functions by promoting Treg cell expansion[53]. In the normal situation, the polyclonal or non-tumor-specific antibodies probably have hardly any antitumor effect. Moreover, in WT mice, a proportion of activated or germinal center B cells would differentiate into PC rapidly and lose their costimulation and tumor-specific antigen presentation abilities in the antitumor process, explaining their relatively weaker tumor response. Nevertheless, the function of various plasma cell subsets and antibodies of different isotypes in human cancers and relevant mouse models warrant future investigations. In any case, the production of such antibodies is likely the result of specific antigen recognition and presentation by B cells.

These studies demonstrate how Blimp-1 deficient B cells exhibit elevated antigen uptake, presentation and costimulation. Transcription factors Pax5, CIITA and Spi-B are directly repressed by Blimp-1[54]. Pax5 activates genes essential for BCR signaling, including Igα, CD19, and BLNK[55]. Blimp-1 suppression of CIITA accounts for the loss of MHC II expression during PC differentiation[56]. Spi-B upregulates CD80 and CD86 in MHC-II hi cells[57]. PU.1 and Spi-B regulate overlapping target genes by binding similar DNA sequences[58]. PU.1 binds CD80 and CD86 promoters to upregulate their expression in DCs[59]. Although these signaling pathways uncover partial molecular mechanisms, cross validation using both models, Blimp-1 BcKO and IgMi, which retain Blimp-1, suggests that inhibition of PC differentiation under tumor challenge results in a general enhancement in activated B cells, including GCB and MBC, and enhanced T cell activation.

CD80, PDL2, and CD73 can identify as many as 5 different memory B cell subsets[43]. The distinct subset of the memory-like B cells we found in this study deserves further investigation. Due to IgM being the most dominant isotype on the CD9 + CD148 + B cells, they may generate IgM+ memory cells and contribute to the antigen-specific memory pool in mice. MBCs can more rapidly respond and differentiate into effector cells after the antigenic reexposure[60]. Mutated IgM+ memory cells have low affinity and can produce GCB in secondary responses triggered by endogenous antigens[61,62], which may help responses to antigenic variants to deal with the complexity of the tumor environment. In addition to tumor in situ presentation by B cells, the higher expression of CD80 on Blimp-1-deficient or IgMi B cells, detected in both tumors and draining LNs, suggest that blocking formation of plasmablasts may also promote the generation of MBCs that contribute to long-lasting anti-tumor efficacy or potential prevention of tumor recurrence.

This study showed that manipulations that inhibit plasma cell differentiation in mice promote an anti-tumor response by favoring B cell antigen presentation to T cells. The response was associated with a unique B cell transcriptional profile. However, we believe the results indicate that such manipulations simply enhance or exaggerate an ongoing natural response. Indications for this are that the restriction of the B cell repertoire in MD4 mice, inhibition of B cell presentation in *H2-Ab1*$^{fl/fl}$ Mb1cre mice, or lack of all B cells in J_H/JCkappa double knockout mice led to enhanced tumor growth, even though these animals were Blimp-1-sufficient. Also supporting this view was the identification of a cluster 2-like population of B cells expressing CD9, CD148, along with CD80, PDL2, and CD73 in control, tumor-bearing mice, though in reduced numbers. Consistent with this, MMTV-PyMT mice showed rapidly improved suppression to spontaneous tumor formation even after short-term treatment with VPA. We acknowledge that the main limitation of our study is that the effects of plasma cell inhibition are only described within discrete mouse models and as yet have no obvious observational data in human; the ability to pharmacologically suppress plasma cell differentiation provides a potential way to validate these concepts in humans. Although FDA-approved and widely used as an antiepileptic and mood stabilizer[63], VPA can cause adverse reactions[64,65]. Moreover, inhibition of Blimp-1 causes cell

proliferation arrest that may be detrimental to tumor-driven clonotype expansion[66]. The development of a more specific plasma cell differentiation blocker should facilitate its evaluation as a target for immunotherapy.

Methods

Mouse strains

IgMi mice were a gift from Dr. M. Shlomchik with permission from Dr. K. Rajewsky. $Jh^{-/-}JCk^{-/-}$ double knockout mice were intercrossed at TSRI from strains $Jh^{-/-}$ and $JCk^{-/-}$[67,68]. *Prdm1*$^{fl/fl}$ (Jax stock no. 008100), *H2-Ab1*$^{fl/fl}$ (Jax stock no. 013181), CD19cre (Jax stock no. 006785), Mb1cre (Jax stock no. 020505), B6.129S7-Rag1^{tm1}Mom/J (Jax stock no. 002216), MD4 (Jax stock no. 002595), and MMTV-PyMT (Jax stock no. 002374) mice were from The Jackson Laboratory. Animals were kept in a special pathogen-free facility at the Scripps Research Institute (TSRI) Immunology Vivarium with housing conditions of 12 light/12 dark cycle at temperatures of 65–75 °F (~18–23 °C) with 40–60% humidity and both female and male mice were used for experiments at 6 to 15 weeks of age. All experiments were approved and monitored by the Animal Care and Use Committee of TSRI.

Tumor inoculation

MC-38 Cell Line purchased from Kerafast, Inc.(from the laboratories of James W. Hodge, PhD, MBA and Jeffrey Schlom, PhD, National Cancer Institute/NIH). B16-F10 cell line (CRL-6475) and LLC1 cell line (CRL-1642) were purchased from ATCC. C57BL/6 mouse primary colonic epithelial cell line (C57-6047) were purchased from Cell Biologics. Tumor cell lines were cultured in DMEM (Corning) supplemented with 10% heat-inactivated Fetal Bovine Serum (FBS, Gemini), 1 × GlutaMax (Gibco), 25 mM HEPES (Gibco), 1 × Non-Essential Amino Acids (Gibco), 4.5 g/l glucose, and sodium pyruvate. Cells were split 1:10 every 3 days, cultured in 37 °C, 5% CO_2 for less than 30 generations since recovery. Cells were trypsinized by TrypLE (Gibco) and washed twice by PBS (Lonza) before inoculation. After cell count and viability were detected by trypan blue staining on Countess™ Automated Cell Counter (ThermoFisher), 1×10^6 cells were subcutaneously (s.c.) injected into the dorsal region of recipient mice. Tumor volume was measured every 3 days until the mouse met protocol endpoints. According to our approved protocol by TSRI, tumor size/burden over 0.5 × 1 × 2 cm is considered to impair the normal function of the mice. For any MMTV-PyMT individual, the tumor volume was calculated as a total volume from measurable primary tumor sites, and any single tumor burden is under control by the euthanizing endpoint guideline. Tumors were weighed and fixed in 10% formalin if needed. For establishing the stable cell line, B16F10 expressing membrane-bound HEL (mHEL), we constructed a G418 selective plasmid, which successively links CMV promoter−membrane signal peptide−HEL−MHC-I tail domain. Plasmid and PEI reagent (1:4) were vortexed quickly and incubated with 1 ml Opti-MEM medium (Gibco) for 10 min at room temperature, followed by addition into 10 ml fresh DMEM medium in a 10 cm dish. Transfected cells were selected under the optimal dose of G418 over 1 week. Monoclonal cell lines were isolated by limiting dilution. The expression of mHEL was detected by flow cytometry. After confirmation of tumor growth in vivo, the B16F10-mHEL stable cell line was cryopreserved and expanded before inoculation.

Flow cytometry analysis

MC38 tumor cells were cultured and transferred s.c. into recipient mice as described above. Tumors were disaggregated mechanically on a 70 µm strainer in PBS buffer containing 2% heat-inactivated FBS. For large tumors, the core of dead cells was removed before the procedure. Tumor-infiltrating lymphocytes (TILs) were pre-isolated by Percoll gradients. 100% Percoll stock solution was prepared by mixing 9 parts of Percoll solution (Cytiva) and 1 part of 10 × PBS, then the stock solution was diluted with 1 × PBS for gradients of 70% and 30%. Before centrifugation (2000 rpm, no brake, 30 min), tumor cell suspensions were loaded in the uppermost layer. The TILs were collected in the band between the 70% and 30% layers. Isolated TILs were washed twice by FACS buffer (1 × PBS containing 5% BSA and 0.5% sodium azide) and filtered through a 40 µm strainer. Before all kinds of staining, the cells were pre-incubated with 0.8–1 µg of anti-mouse CD16/CD32 or Fc blocker per 100 µL for 10 min at 4 °C to block non-specific Fc-mediated interactions. Single-cell suspensions were stained with the following antibodies: CD138-BV421, B220-FITC, CD38-PE/Cy7, CD86-APC, CD80-PerCP/Cy5.5, I-A/I-E-BV421, CD19-PE/Cy7, CD69-PE, CD44-FITC, CD8a-Bv421, Tim-3-PE/Cy7, CD4-PerCP/Cy5.5, PD-1-APC, CD8a-AF488, IFNγ-APC, GzmB-PE/Cy7, F4/80-FITC, CD86-AF700, PDL2-PE/Dazzle594, IgM-PE/Cy7, IgD-FITC, CD73-BV605, CD80-PE/Dazzle594 (Biolegend), GL-7-PE, CD95-AF647, CD62L-PE, I-Ab-FITC, CD11b-BUV661, CD20-BV711, CD19-BV480, B220-BUV496, CD148-BV421, IgD-BV711 (BD Biosciences), Foxp3-PE/Cy7 (ThermoFisher). We provide the dilution of antibodies used under "ratio", in between "Clone#" and "Vendor" information, in the reporting summary document. CD9 was stained by biotin-conjugated primary Ab followed by Streptavidin-BV650. CXCR5 and mHEL was stained by primary Ab and biotin-conjugated second Ab, followed by Streptavidin-APC. Titrated concentrations AC-1 or AC-2 were used to stain 0.3–0.5 million target cells on ice for 45 min, then the cells were washed twice. This was followed by staining with biotin-conjugated anti-human IgG on ice for 45 min, then washed twice. Finally, the cells were stained with streptavidin-APC on ice for 30 min. Dead cells were excluded using viability dye eFluor™ 780 (ThermoFisher). For intracellular stainings, cells were stimulated with 1 × stimulation cocktail (ThermoFisher) and 1 × protein transport inhibitor (BD Biosciences) for 5 h at 37 °C. After surface staining, cells were fixed by 4% PFA, followed by permeabilization and staining with Perm/Wash™ Buffer (BD Biosciences). For intranuclear staining, the Foxp3 Fixation/Permeabilization solution (TONBO Biosciences) was used after surface staining. All samples were acquired on BD LSR2 flow cytometer (BD Biosciences), or Aurora spectral flow cytometry (Cytek Biosciences) and data were analyzed using Flowjo software (v10).

Sample preparation for single-cell RNA sequencing libraries and data analysis

MC38 tumor cells were cultured and transferred s.c. into recipient mice as described above. On DPI 18, inoculated MC38 tumors were collected from 11 recipients in each group. Immune cells were enriched by percoll gradients first, then sorted as single B220+ cells and single CD138+ cells from living cells using the Sony MA900 cell sorter. Good yield of cDNA was obtained from the combination of B220+ and CD138+ cells and all quality control checks passed on the Bioanalyzer; then samples were processed with the VDJ and GEX library preparations. The FASTQ files of the sequencing data were analyzed by RStudio (4.2.2). *Seurat* R package (4.3.0)[69] were used to process and integrate analysis across data sets. Genes that expressed in fewer than 3 cells or cells that expressed fewer than 200 genes were excluded. Most variable genes were identified using *FindVariableFeatures* function by setting feature numbers as 2000. UMAP 2D visualization were created from the principal component analysis matrix. Clustering was performed using *FindClusters* with resolution 0.5 for default analysis. Differential gene expressions were analyzed by using *FindMarkers* function in *Seurat* R package. *scRepertoire* R package (1.8.0)[70,71] was used in general analysis of single cell clonotype and assist in the analysis of V(D)J sequencing interaction with mRNA expression data using *Seurat*. The construction of sub-clustering B cells *Seurat* object was imported into *Monocle2* R package (1.3.1)[72] for single-cell trajectory and pseudotime analysis. *ClusterProfiler* R package(4.6.2)[73] was used for gene functional enrichment analysis. ORA results were shown by dot plot visualization.

Serum transfer

MC38 tumor-bearing C57BL/6 mice were bled at 21 days post-inoculation. Serum was harvested after centrifugation at 4 °C, diluted 3 times with PBS and designated as Sera-21 without heat-inactivation (w/o HI) or serum was harvested and incubated at 56 °C for 0.5 h to inactivate complement. The heat-inactivated serum was divided equally into two parts. One part was diluted 3 times with PBS (Sera-21 with heat inactivation), while the other part was incubated while rotating for 1 h with a mixture of Protein G Sepharose™ (Cytiva) and Capto™ L (Cytiva) to capture all Ig isotypes. After washing the beads with PBS, elution buffer pH 2.8 (Pierce Biotechnology) was used to elute the Ig molecules from beads. The Ig Capture solution was neutralized by 2 M Tris pH 9.0 and diluted 3 times with PBS. Seven days before serum transfer, MC38 tumor cells were s.c. injected into *Prdm1*$^{fl/fl}$ CD19cre and *Prdm1*$^{fl/fl}$ mice; B16F10-mHEL cells were s.c. inoculated into MD4− mice or MD4+ mice. Sera-0 were collected from C57BL/6 mice without tumor burden. Sera-HEL was obtained by injection of a mixture of 50 µg HEL and 5 µg LPS into the mouse footpads 6 days before serum collection. Mice received 0.3 ml i.v. of Sera-0 or Sera-HEL dilutions, respectively, on days 7, 10, 13, and total transferred anti-HEL antibodies equal to 18 µg and 36 µg.

Enzyme-linked immunosorbent assay (ELISA)

Tumor-induced immunoglobulins in serum were measured by sandwich ELISA and quantified using a mouse immunoglobulin panel (SouthernBiotech), including purified mouse IgA, IgG1, IgG2b, IgG2c, IgG3, and IgM. Serum samples were collected retroorbitally under anesthesia on day 15 or 21 post-inoculation of MC38 tumor, diluted in an equal volume of glycerol, and stored at −20 °C. 96-well plates (Genesee Scientific) were coated with 5 µg/ml capture antibody at 4 °C overnight. Plates were washed with PBST (PBS containing 0.05% Tween-20) and incubated with PBS containing 1% bovine serum albumin (BSA, Biotium) at room temperature for 2 h to block non-specific binding sites. After washing the plate with PBST, serum samples were diluted in ChonBlock™ buffer (Chondrex) and incubated in wells at room temperature for 1 h with gentle shaking. HRP-labeled detection antibodies were diluted in ChonBlock™ buffer (Chondrex) and added to each well after washing the plate with PBST, followed by incubation at room temperature for 1 h with gentle shaking. The plate was washed multiple times with PBST, followed by the addition of 0.1 ml TMB substrate solution to each well and incubated at room temperature for 10–15 min. Reaction was stopped with 0.1 ml 2 M sulfuric acid. Absorbance was measured at 450 nm and 630 nm (background absorption). Serum titers of anti-HEL antibody were measured by direct ELISA and standardized using serial dilution of purified mouse IgM (SouthernBiotech). Serum samples were collected from MD4+ mice on day 18 post-inoculation of specific tumor cells, diluted in an equal volume of glycerol, and stored at −20 °C. 96-well plates (Genesee Scientific) were coated with 5 µg/ml HEL (Roche) in PBS overnight at 4 °C. Coated plates were blocked with PBS containing 3% BSA (Biotium) at room temperature for 2 h, followed by washing with PBST. Serum samples were diluted in ChonBlock™ buffer (Chondrex) before use. Diluted sera and standard were added to blocked plates and incubated at 4 °C overnight with gentle shaking. Plates were washed with PBST, added with diluted HRP-labeled goat anti-mouse IgM in ChonBlock™ buffer (Chondrex), and incubated at room temperature for 1 h with gentle shaking. Plates were then washed with PBST, followed by incubation with TMB substrate reaction and measurement of absorbance.

VPA and antibody treatment

For VPA treatment, VPA sodium salt (Sigma-Aldrich) was dissolved in drinking water at 0.4% or 0.8% w/v, concentrations sufficient to maintain a stable serum level of VPA in mice[44]. VPA-containing drinking water was given to animals on the day of tumor injection and ensured sufficient water until the end of tumor volume records. MMTV-PyMT female mice started their 0.8% (w/v) VPA treatment at the age of 6 weeks, and multiple breast tumors were calculated as sum until experimental endpoints. For MHC II blockade, tumor-bearing mice were treated intraperitoneally on days 0, 3, 7, 10, 13, 16 with 0.1 mg anti-mouse MHC Class II (I-A/I-E) antibody (clone M5/114, Bio X Cell) or isotype control antibody.

Statistics

GraphPad Prism 8 software (Graphpad Software) was used for statistical analysis. The statistical significance of differences between two groups was calculated with two-tailed unpaired *t*-tests, and ANOVA analysis or two-tailed unpaired multiple *t*-tests with Holm–Sidak's correction were used to compare differences across multiple experimental groups (NS, $P > 0.05$; *, $P < 0.05$; **, $P < 0.01$; ***, $P < 0.001$; ****, $P < 0.0001$). Error bars represent SEM.

Reporting summary

Further information on research design is available in the Nature Portfolio Reporting Summary linked to this article.

Data availability

Source data are provided with this paper. The Single-cell RNA-seq data and VDJseq data generated in this study have been deposited in the Gene Expression Omnibus (GEO) database under accession code GSE289410. The remaining data are available within the Article, Supplementary Information or Source Data file. Source data are provided with this paper.

Code availability

The code used to generate the figures is available[74] in the following repository on GitHub: https://github.com/NemazeeLab/Blimp1KOvsCtrl.git.

References

1. Sharonov, G. V., Serebrovskaya, E. O., Yuzhakova, D. V., Britanova, O. V. & Chudakov, D. M. B cells, plasma cells and antibody repertoires in the tumour microenvironment. *Nat. Rev. Immunol.* **20**, 294–307 (2020).
2. Laumont, C. M. & Nelson, B. H. B cells in the tumor microenvironment: multi-faceted organizers, regulators, and effectors of anti-tumor immunity. *Cancer Cell* **41**, 466–489 (2023).
3. Reuschenbach, M., von Knebel Doeberitz, M. & Wentzensen, N. A systematic review of humoral immune responses against tumor antigens. *Cancer Immunol. Immunother.* **58**, 1535–1544 (2009).
4. Zhang, X., Liu, M., Zhang, X., Wang, Y. & Dai, L. Autoantibodies to tumor-associated antigens in lung cancer diagnosis. *Adv. Clin. Chem.* **103**, 1–45 (2021).
5. Oshima, Y. et al. NY-ESO-1 autoantibody as a tumor-specific biomarker for esophageal cancer: screening in 1969 patients with various cancers. *J. Gastroenterol.* **51**, 30–34 (2016).
6. Wieland, A. et al. Defining HPV-specific B cell responses in patients with head and neck cancer. *Nature* **597**, 274–278 (2021).
7. Nielsen, J. S. et al. CD20+ tumor-infiltrating lymphocytes have an atypical CD27- memory phenotype and together with CD8+ T cells promote favorable prognosis in ovarian cancer. *Clin. Cancer Res.* **18**, 3281–3292 (2012).
8. Garaud, S. et al. Tumor infiltrating B-cells signal functional humoral immune responses in breast cancer. *JCI Insight* **4**, e129641 (2019).
9. Schaafsma, E., Jiang, C. & Cheng, C. B cell infiltration is highly associated with prognosis and an immune-infiltrated tumor microenvironment in neuroblastoma. *J. Cancer Metastasis Treat.* **7**, 34 (2021).
10. Harris, R. J. et al. Tumor-infiltrating B lymphocyte profiling identifies IgG-biased, clonally expanded prognostic phenotypes in triple-negative breast cancer. *Cancer Res.* **81**, 4290–4304 (2021).

11. Biswas, S. et al. IgA transcytosis and antigen recognition govern ovarian cancer immunity. *Nature* **591**, 464–470 (2021).
12. Kotsiliti, E. et al. Intestinal B cells license metabolic T-cell activation in NASH microbiota/antigen-independently and contribute to fibrosis by IgA-FcR signalling. *J. Hepatol.* **79**, 296–313 (2023).
13. Ouyang, F. Z. et al. Dendritic cell-elicited B-cell activation fosters immune privilege via IL-10 signals in hepatocellular carcinoma. *Nat. Commun.* **7**, 13453 (2016).
14. Yang, S. Y. et al. Characterization of organ-specific regulatory B cells using single-cell RNA sequencing. *Front. Immunol.* **12**, 711980 (2021).
15. Affara, N. I. et al. B cells regulate macrophage phenotype and response to chemotherapy in squamous carcinomas. *Cancer Cell* **25**, 809–821 (2014).
16. Wei, Y. et al. Plasma cell polarization to the immunoglobulin G phenotype in hepatocellular carcinomas involves epigenetic alterations and promotes hepatoma progression in mice. *Gastroenterology* **156**, 1890–1904 e1816 (2019).
17. Helmink, B. A. et al. B cells and tertiary lymphoid structures promote immunotherapy response. *Nature* **577**, 549–555 (2020).
18. Candolfi, M. et al. B cells are critical to T-cell-mediated antitumor immunity induced by a combined immune-stimulatory/conditionally cytotoxic therapy for glioblastoma. *Neoplasia* **13**, 947–960 (2011).
19. Cui, C. et al. Neoantigen-driven B cell and CD4 T follicular helper cell collaboration promotes anti-tumor CD8 T cell responses. *Cell* **184**, 6101–6118 e6113 (2021).
20. Ron, Y. & Sprent, J. T cell priming in vivo: a major role for B cells in presenting antigen to T cells in lymph nodes. *J. Immunol.* **138**, 2848–2856 (1987).
21. Crawford, A., Macleod, M., Schumacher, T., Corlett, L. & Gray, D. Primary T cell expansion and differentiation in vivo requires antigen presentation by B cells. *J. Immunol.* **176**, 3498–3506 (2006).
22. Lanzavecchia, A. Antigen-specific interaction between T and B cells. *Nature* **314**, 537–539 (1985).
23. Rock, K. L., Benacerraf, B. & Abbas, A. K. Antigen presentation by hapten-specific B lymphocytes. I. Role of surface immunoglobulin receptors. *J. Exp. Med.* **160**, 1102–1113 (1984).
24. Getahun, A. & Cambier, J. C. Non-antibody-secreting functions of B cells and their contribution to autoimmune disease. *Annu. Rev. Cell Dev. Biol.* **35**, 337–356 (2019).
25. Lund, F. E. & Randall, T. D. Effector and regulatory B cells: modulators of CD4+ T cell immunity. *Nat. Rev. Immunol.* **10**, 236–247 (2010).
26. Crotty, S., Johnston, R. J. & Schoenberger, S. P. Effectors and memories: Bcl-6 and Blimp-1 in T and B lymphocyte differentiation. *Nat. Immunol.* **11**, 114–120 (2010).
27. Lin, Y., Wong, K. & Calame, K. Repression of c-myc transcription by Blimp-1, an inducer of terminal B cell differentiation. *Science* **276**, 596–599 (1997).
28. Shapiro-Shelef, M. et al. Blimp-1 is required for the formation of immunoglobulin secreting plasma cells and pre-plasma memory B cells. *Immunity* **19**, 607–620 (2003).
29. Waisman, A. et al. IgG1 B cell receptor signaling is inhibited by CD22 and promotes the development of B cells whose survival is less dependent on Ig alpha/beta. *J. Exp. Med.* **204**, 747–758 (2007).
30. Waisman, A., Croxford, A. L. & Demircik, F. New tools to study the role of B cells in cytomegalovirus infections. *Med. Microbiol. Immunol.* **197**, 145–149 (2008).
31. Wang, W. et al. Ribosomal proteins and human diseases: pathogenesis, molecular mechanisms, and therapeutic implications. *Med. Res. Rev.* **35**, 225–285 (2015).
32. Allan, L. L. et al. Apolipoprotein-mediated lipid antigen presentation in B cells provides a pathway for innate help by NKT cells. *Blood* **114**, 2411–2416 (2009).
33. Damdinsuren, B., Dement-Brown, J., Li, H. & Tolnay, M. B cell receptor induced Fc receptor-like 5 expression is mediated by multiple signaling pathways converging on NF-kappaB and NFAT. *Mol. Immunol.* **73**, 112–121 (2016).
34. Smith, K. G. & Clatworthy, M. R. FcgammaRIIB in autoimmunity and infection: evolutionary and therapeutic implications. *Nat. Rev. Immunol.* **10**, 328–343 (2010).
35. Zhang, W. et al. Excessive CD11c(+)Tbet(+) B cells promote aberrant T(FH) differentiation and affinity-based germinal center selection in lupus. *Proc. Natl. Acad. Sci. USA* **116**, 18550–18560 (2019).
36. Rubtsov, A. V. et al. CD11c-expressing B cells are located at the T Cell/B cell border in spleen and are potent APCs. *J. Immunol.* **195**, 71–79 (2015).
37. Morgan, D. & Tergaonkar, V. Unraveling B cell trajectories at single cell resolution. *Trends Immunol.* **43**, 210–229 (2022).
38. Kennedy, D. E. et al. Novel specialized cell state and spatial compartments within the germinal center. *Nat. Immunol.* **21**, 660–670 (2020).
39. Ye, J., Ma, N., Madden, T. L. & Ostell, J. M. IgBLAST: an immunoglobulin variable domain sequence analysis tool. *Nucleic Acids Res.* **41**, W34–W40 (2013).
40. Goodnow, C. C. et al. Altered immunoglobulin expression and functional silencing of self-reactive B lymphocytes in transgenic mice. *Nature* **334**, 676–682 (1988).
41. Phan, T. G. et al. B cell receptor-independent stimuli trigger immunoglobulin (Ig) class switch recombination and production of IgG autoantibodies by anergic self-reactive B cells. *J. Exp. Med.* **197**, 845–860 (2003).
42. Greenwald, R. J., Freeman, G. J. & Sharpe, A. H. The B7 family revisited. *Annu Rev. Immunol.* **23**, 515–548 (2005).
43. Zuccarino-Catania, G. V. et al. CD80 and PD-L2 define functionally distinct memory B cell subsets that are independent of antibody isotype. *Nat. Immunol.* **15**, 631–637 (2014).
44. White, C. A. et al. Histone deacetylase inhibitors upregulate B cell microRNAs that silence AID and Blimp-1 expression for epigenetic modulation of antibody and autoantibody responses. *J. Immunol.* **193**, 5933–5950 (2014).
45. Shen, M., Sun, Q., Wang, J., Pan, W. & Ren, X. Positive and negative functions of B lymphocytes in tumors. *Oncotarget* **7**, 55828–55839 (2016).
46. Wennhold, K. et al. CD86(+) antigen-presenting B cells are increased in cancer, localize in tertiary lymphoid structures, and induce specific T-cell responses. *Cancer Immunol. Res.* **9**, 1098–1108 (2021).
47. Bruno, T. C. et al. Antigen-presenting intratumoral B cells affect CD4(+) TIL phenotypes in non-small cell lung cancer patients. *Cancer Immunol. Res.* **5**, 898–907 (2017).
48. Petitprez, F. et al. B cells are associated with survival and immunotherapy response in sarcoma. *Nature* **577**, 556–560 (2020).
49. Jiang, Q. et al. CD19(+) tumor-infiltrating B-cells prime CD4(+) T-cell immunity and predict platinum-based chemotherapy efficacy in muscle-invasive bladder cancer. *Cancer Immunol. Immunother.* **68**, 45–56 (2019).
50. Zirakzadeh, A. A. et al. Doxorubicin enhances the capacity of B cells to activate T cells in urothelial urinary bladder cancer. *Clin. Immunol.* **176**, 63–70 (2017).
51. Kirk, A. D., Turgeon, N. A. & Iwakoshi, N. N. B cells and transplantation tolerance. *Nat. Rev. Nephrol.* **6**, 584–593 (2010).
52. Newick, K., O'Brien, S., Moon, E. & Albelda, S. M. CAR T cell therapy for solid tumors. *Annu. Rev. Med.* **68**, 139–152 (2017).
53. Pinto, D. et al. A functional BCR in human IgA and IgM plasma cells. *Blood* **121**, 4110–4114 (2013).
54. Minnich, M. et al. Multifunctional role of the transcription factor Blimp-1 in coordinating plasma cell differentiation. *Nat. Immunol.* **17**, 331–343 (2016).
55. Schebesta, A. et al. Transcription factor Pax5 activates the chromatin of key genes involved in B cell signaling, adhesion, migration, and immune function. *Immunity* **27**, 49–63 (2007).

56. Piskurich, J. F. et al. BLIMP-I mediates extinction of major histocompatibility class II transactivator expression in plasma cells. *Nat. Immunol.* **1**, 526–532 (2000).
57. Akiyama, N. et al. Limitation of immune tolerance-inducing thymic epithelial cell development by Spi-B-mediated negative feedback regulation. *J. Exp. Med.* **211**, 2425–2438 (2014).
58. Garrett-Sinha, L. A. et al. PU.1 and Spi-B are required for normal B cell receptor-mediated signal transduction. *Immunity* **10**, 399–408 (1999).
59. Kanada, S. et al. Critical role of transcription factor PU.1 in the expression of CD80 and CD86 on dendritic cells. *Blood* **117**, 2211–2222 (2011).
60. Bhattacharya, D. et al. Transcriptional profiling of antigen-dependent murine B cell differentiation and memory formation. *J. Immunol.* **179**, 6808–6819 (2007).
61. Pape, K. A., Taylor, J. J., Maul, R. W., Gearhart, P. J. & Jenkins, M. K. Different B cell populations mediate early and late memory during an endogenous immune response. *Science* **331**, 1203–1207 (2011).
62. Dogan, I. et al. Multiple layers of B cell memory with different effector functions. *Nat. Immunol.* **10**, 1292–1299 (2009).
63. Phiel, C. J. et al. Histone deacetylase is a direct target of valproic acid, a potent anticonvulsant, mood stabilizer, and teratogen. *J. Biol. Chem.* **276**, 36734–36741 (2001).
64. Pagali, S., Edquist, C. & O'Rourke, N. Managing valproic acid toxicity-related hyperammonaemia: an unpredicted course. *BMJ Case Rep.* **14**, e241547 (2021).
65. Nanau, R. M. & Neuman, M. G. Adverse drug reactions induced by valproic acid. *Clin. Biochem.* **46**, 1323–1338 (2013).
66. Shapiro-Shelef, M. & Calame, K. Regulation of plasma-cell development. *Nat. Rev. Immunol.* **5**, 230–242 (2005).
67. Chen, J. et al. Immunoglobulin gene rearrangement in B cell deficient mice generated by targeted deletion of the JH locus. *Int. Immunol.* **5**, 647–656 (1993).
68. Chen, J. et al. B cell development in mice that lack one or both immunoglobulin kappa light chain genes. *EMBO J.* **12**, 821–830 (1993).
69. Butler, A., Hoffman, P., Smibert, P., Papalexi, E. & Satija, R. Integrating single-cell transcriptomic data across different conditions, technologies, and species. *Nat. Biotechnol.* **36**, 411–420 (2018).
70. Borcherding, N., Bormann, N. L. & Kraus, G. scRepertoire: an R-based toolkit for single-cell immune receptor analysis. *F1000Res.* **9**, 47 (2020).
71. Wu, T. D. et al. Peripheral T cell expansion predicts tumour infiltration and clinical response. *Nature* **579**, 274–278 (2020).
72. Qiu, X. et al. Reversed graph embedding resolves complex single-cell trajectories. *Nat. Methods* **14**, 979–982 (2017).
73. Wu, T. et al. clusterProfiler 4.0: a universal enrichment tool for interpreting omics data. *Innovation (Camb.)* **2**, 100141 (2021).
74. Li, Y. et al. Blocking plasma cell fate enhances antigen-specific presentation by B cells to boost anti-tumor immunity. *GitHub* https://doi.org/10.5281/zenodo.15042652 (2025).

Acknowledgements

This study was supported by National Institutes of Health (R01AI137252 to C.X. and D.N.). We thank members of Xiao and Nemazee laboratories for discussion, and J.X. from Xiamen University for critical suggestions. We thank Mark Shlomchik for making the IgMi mice available, Steven Robert Head and Tony Mondala from the Scripps Genomics Core for assistance with scRNAseq, and Padmaja Natarajan and Aishwarya Sundaresan from the Scripps Center for Computational Biology and Bioinformatics for assistance with sequencing analysis and data deposition.

Author contributions

Y.L. designed and performed the experiments, analyzed data, and contributed to the writing of the manuscript; R.B. and J.T.T. participated in some experiments and provided technical support to maintain mouse colonies. T.R.B. provided mice for experiments. L.P. designed and constructed the plasmids; F.L. helped with the maintenance of mouse colonies; Z.Z. and Y.S. collected patient samples and contributed with human relevance. Y.L., Z.H., C.X., and D.N. conceived and designed this study. The initial discovery was made by Y.L. in the Xiao lab, and the study was continued in the Nemazee lab due to the departure of C.X. from The Scripps Research Institute in 2021. Y.L., C.X., and D.N. wrote the manuscript with contributions from other authors.

Competing interests

The authors declare no competing interests.

Additional information

Supplementary information The online version contains supplementary material available at https://doi.org/10.1038/s41467-025-59622-4.

Correspondence and requests for materials should be addressed to Changchun Xiao or David Nemazee.

Peer review information *Nature Communications* thanks Bo Sun, Xiaoming Zhang and the other anonymous reviewer(s) for their contribution to the peer review of this work. A peer review file is available.